Lipin-2 regulates NLRP3 inflammasome by affecting $P2X_7$ receptor activation

Gema Lordén,[1,3] Itziar Sanjuán-García,[1,3] Nagore de Pablo,[1,3] Clara Meana,[1,3] Inés Alvarez-Miguel,[1,2] M. Teresa Pérez-García,[1,2] Pablo Pelegrín,[4] Jesús Balsinde,[1,3] and María A. Balboa[1,3]

[1]Instituto de Biología y Genética Molecular, Consejo Superior de Investigaciones Científicas and [2]Departamento de Fisiología, Facultad de Medicina, Universidad de Valladolid, 47003 Valladolid, Spain
[3]Centro de Investigación Biomédica en Red de Diabetes y Enfermedades Metabólicas Asociadas, 28029 Madrid, Spain
[4]Molecular Inflammation Group, Murcia Biomedical Research Institute, Hospital Virgen de la Arrixaca, Carretera Buenavista, 30120 Murcia, Spain

Mutations in human *LPIN2* produce a disease known as Majeed syndrome, the clinical manifestations of which are ameliorated by strategies that block IL-1β or its receptor. However the role of lipin-2 during IL-1β production remains elusive. We show here that lipin-2 controls excessive IL-1β formation in primary human and mouse macrophages by several mechanisms, including activation of the inflammasome NLRP3. Lipin-2 regulates MAPK activation, which mediates synthesis of pro–IL-1β during inflammasome priming. Lipin-2 also inhibits the activation and sensitization of the purinergic receptor P2X7 and K^+ efflux, apoptosis-associated speck-like protein with a CARD domain oligomerization, and caspase-1 processing, key events during inflammasome activation. Reduced levels of lipin-2 in macrophages lead to a decrease in cellular cholesterol levels. In fact, restoration of cholesterol concentrations in cells lacking lipin-2 decreases ion currents through the P2X7 receptor, and downstream events that drive IL-1β production. Furthermore, lipin-2–deficient mice exhibit increased sensitivity to high lipopolysaccharide doses. Collectively, our results unveil lipin-2 as a critical player in the negative regulation of NLRP3 inflammasome.

INTRODUCTION

Inflammasomes are large intracellular multiprotein complexes that are key players in host defense during innate immune responses against pathogen microorganisms, and also in the development of inflammatory disorders. Inflammasomes are believed to assemble after cellular exposure to pathogens and danger signals, orchestrating innate immune responses through activation of caspase-1, leading to the maturation of proinflammatory cytokines to produce IL-1β and IL-18. The inflammasome NLRP3 is the best characterized to date (Hoffman et al., 2001; Elliott and Sutterwala, 2015; Man and Kanneganti, 2015). It is composed of a pattern recognition receptor that belongs to the Nod-like receptor family (NLR), the adaptor protein apoptosis-associated speck-like protein with a CARD domain (ASC) and caspase-1. Its activation and assembly need two signals. The first signal, also known as priming, leads to transcription of genes encoding NLRP3 and pro–IL-1β and occurs through activation of various receptors, such as TLRs (Bauernfeind et al., 2009). The second signal activates inflammasome assembly, resulting in the catalytic processing of pro–caspase-1 into its enzymatically active form. NLRP3 inflammasome is activated by a wide range of stimuli, such as bacterial and viral pathogens, pore-forming toxins, lipids, crystals, vaccine adjuvants, and stress cellular signals such as ATP.

Extracellular ATP is sensed by immune cells as a danger signal, and has been widely used as an inflammasome inducer. ATP exerts its biological action by binding to purinergic receptors such as $P2X_7$ ($P2X_7R$; Surprenant et al., 1996; Mariathasan et al., 2006; Di Virgilio, 2015). $P2X_7R$ is a nonselective cationic channel abundantly expressed in macrophages, whose activation promotes the opening of a pore that allows an influx of Na^+ and Ca^{2+} into the cytosol and the concomitant efflux of K^+ (Buisman et al., 1988). Thus, binding of ATP at high concentrations (millimolar range) to $P2X_7R$ promotes a decrease in intracellular K^+ levels that triggers inflammasome assembly (Perregaux and Gabel, 1994; Mariathasan et al., 2006). However, in response to a prolonged exposure to agonists, $P2X_7R$ undergoes sensitization, resulting in increased current amplitudes and dilation of the pore, which can be permeable to large (≤800 D) inorganic and organic molecules (Surprenant et al., 1996; Di Virgilio, 2015). Because the latter process could be damaging to the cell, the function of $P2X_7R$ needs to be tightly regulated, and finding cellular brakes for this receptor could be of special

Correspondence to María A. Balboa: mbalboa@ibgm.uva.es

Abbreviations used: ASC, apoptosis-associated speck-like protein with a CARD domain; BMDM, BM-derived macrophage; LDH, lactate dehydrogenase; MCD, methyl-β-cyclodextrin; PI, propidium iodide.

The Rockefeller University Press $30.00
J. Exp. Med. 2017 Vol. 214 No. 2 511–528
https://doi.org/10.1084/jem.20161452

interest both to restrain IL-1β production in inflammatory diseases, and also to stop undesired cell death.

Dysregulation of the NLRP3 inflammasome is associated with a wide spectrum of autoinflammatoy diseases, characterized by recurrent fever and unprovoked episodes of inflammation, in which the monocyte-macrophage is the dysfunctional cell (Holzinger et al., 2015). Usually, blockade of IL-1β improves clinical symptoms in patients, whereas TNF neutralization, a highly effective therapy for autoimmune diseases, poorly controls autoinflammatory disorders (Quartier et al., 2011). From all autoinflammatory diseases characterized to date, it is interesting to highlight the Majeed syndrome, the molecular defect of which does not reside in mutations of genes related to inflammasome proteins or IL-1 biology (Majeed et al., 1989). This syndrome is an autosomal recessive disease generated by mutations in the *LPIN2* gene that encodes for lipin-2, a key enzyme in lipid metabolism (Ferguson et al., 2005; Al-Mosawi et al., 2007). Lipin-2 is a member of a family of proteins, the lipins, which catalyze the enzymatic conversion of phosphatidic acid to diacylglycerol in a Mg^{2+}-dependent manner (Péterfy et al., 2001). By regulating these two important cellular lipids, lipins can influence triacylglycerol and phospholipid biosynthetic pathways (Stein and Shapiro, 1957; Han et al., 2006; Kok et al., 2012). Lipins have been found in macrophages, where lipin-1 and lipin-2 seem to play opposite roles during inflammatory responses (Valdearcos et al., 2011, 2012; Meana et al., 2014; Navratil et al., 2015).

Five independent *LPIN2* mutations are known to cause Majeed syndrome (Ferguson et al., 2005; Al-Mosawi et al., 2007; Herlin et al., 2013; Rao et al., 2016). Four of these mutations produce premature stop codons, and the last of them is a point mutation of a highly conserved residue among lipins (Ser^{734}), that eliminates lipin-2 PAP activity but not its ability to associate with microsomes (Donkor et al., 2009). Majeed syndrome may start very early in life (weeks) and its phenotype includes chronic recurrent multifocal osteomyelitis, congenital dyserythropoietic anemia, recurrent fevers and inflammation of the bone and skin (Majeed et al., 1989; Ferguson et al., 2005; Al-Mosawi et al., 2007). In Majeed syndrome patients, IL-1β blockade is accompanied by symptomatic improvement on clinical and biological parameters (Herlin et al., 2013). These data strongly support the idea that IL-1β plays a key role in the development of the disease. The underlying mechanisms by which mutations in *LPIN2* cause this syndrome are unknown. Because of the involvement of IL-1β in this process, we hypothesized that lipin-2 might be involved in its production and, therefore, in the regulation of inflammasome activity. Accordingly, in the present study we have examined the role of lipin-2 in inflammasome activation and IL-1β production in primary BM-derived macrophages (BMDMs) from *Lpin2*$^{-/-}$ mice and primary human macrophages made deficient in lipin-2. We found that lipin-2 controls both the priming and activation phase of the inflammasome NLRP3. Specifically, lipin-2 limits TLR4 activation and maintains a proper lipid environment for $P2X_7R$ that inhibits its overactivation. These results expand the role of lipin-2 as an important innate immune regulator.

RESULTS

Lipin-2 restrains IL-1β production by NLRP3 inflammasome

Patients with mutations in the *LPIN2* gene have increased levels of IL-1β in serum (Herlin et al., 2013). However, it is not known whether mutated lipin-2 has a direct effect on IL-1β–producing cells. To answer this question, lipin-2 expression was knocked-down by siRNA technology in human macrophages. IL-1β production was triggered by classical activation of NLRP3 inflammasome, i.e., LPS as the priming signal and ATP as the second signal. We found that decreased cellular levels of lipin-2 resulted in a significant increase in the production of IL-1β in these cells (Fig. 1 A). To further characterize this finding, we evaluated the production of the cytokine in BMDMs from *Lpin2*$^{-/-}$ mice, where the absence of the enzyme is complete. Again, these cells had a larger capacity for producing IL-1β than BMDMs generated from WT animals (Fig. 1, B and D). Furthermore, elimination of the enzyme in the murine cell line RAW264.7 also promoted increased IL-1β production with respect to control cells (Fig. 1 C). We then investigated whether NLRP3 inflammasome contributed to those observed effects. Fig. 1 E shows that absence of key elements of the NLRP3 inflammasome, such as the NLRP3 sensor, the ASC adapter, or the effector protein caspase-1 in BMDM cells, completely abrogated the cell's capacity to generate IL-1β, either in the presence or absence of lipin-2. These data suggest that the overstimulating effect of lipin-2 on IL-1β production works through the NLRP3 inflammasome.

Lipin-2 ameliorates TLR4 signaling

To evaluate whether lipin-2 is implicated in TLR4 activation, we analyzed first mRNA levels for *Tnf*, a gene classically up-regulated by LPS. We found that the mRNA levels for this gene, as well as the levels of secreted TNF were higher in BMDMs from *Lpin2*$^{-/-}$ animals than in WT cells (Fig. 2, A and B). By analyzing *Il1b* mRNA and pro–IL-1β we also observed the same behavior (Fig. 2, C and D). Importantly, human macrophages made deficient in lipin-2 also produced higher levels of TNF and had higher levels of *IL1B* mRNA (Fig. 2, B and C).

We then studied whether, during LPS treatment, MAPKs phosphorylation was also affected by lipin-2. The results demonstrated that BMDMs from *Lpin2*$^{-/-}$ animals had increased phosphorylation levels for ERK, JNK, and p38, especially after 30 min of stimulation (Fig. 2 E). Next, the impact of these kinases on *Il1b* mRNA production was evaluated by using specific inhibitors. Inhibition of p38 (SB203580) completely abolished *Il1b* mRNA up-regulation independently of the level of lipin-2, whereas JNK inhibition (SP600125) completely blocked the overproduction of the cytokine generated by lipin-2–deficient cells. Similarly,

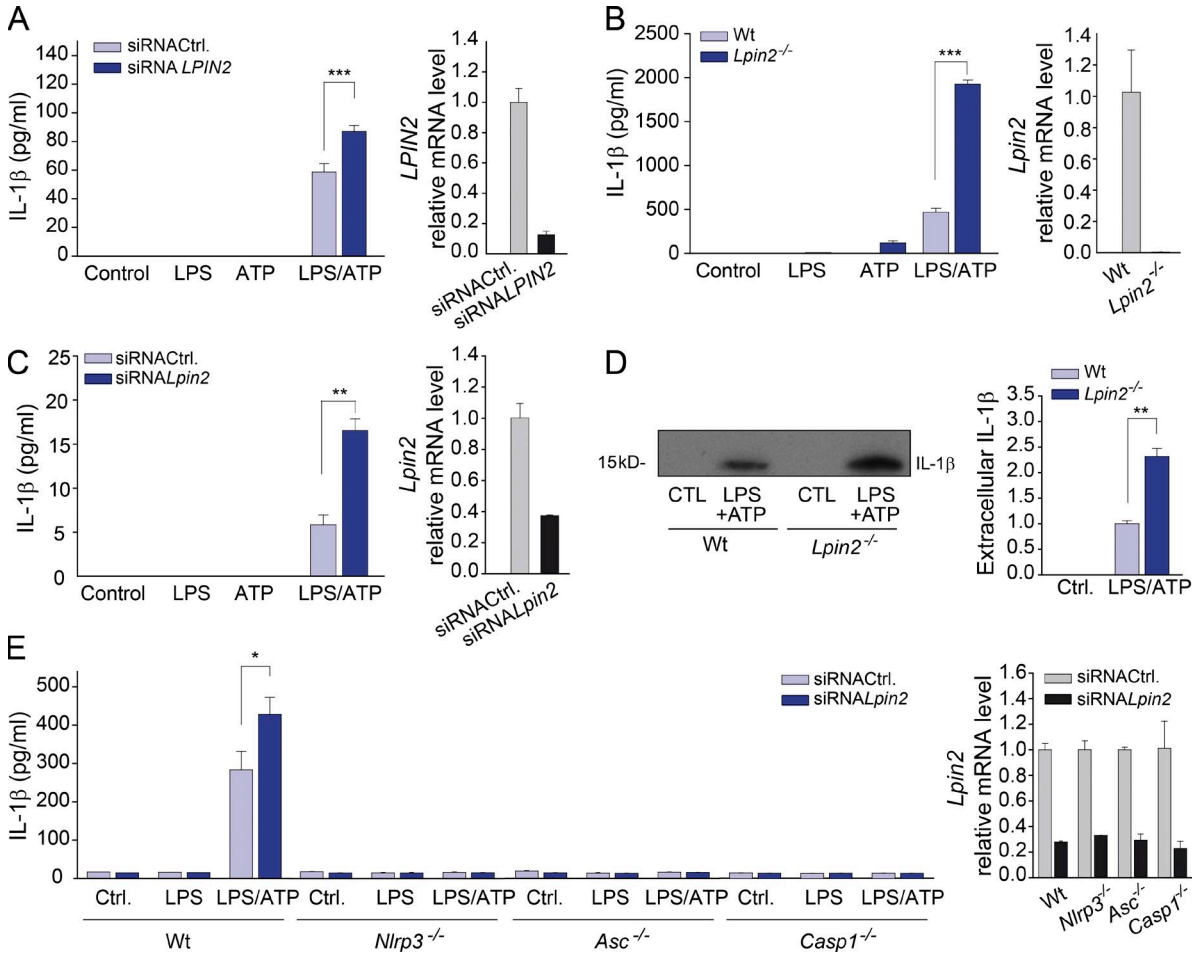

Figure 1. **The effect of lipin-2 on IL-1β production by murine and human macrophages.** IL-1β presence in supernatants from primary human macrophages (A), BMDMs from WT and *Lpin2*$^{-/-}$ mice (B and D), or RAW264.7 cells (C) stimulated with 200 ng/ml LPS for 4 h, 2 mM ATP for 40 min, or both, as indicated, were quantified by specific ELISAs. (A–C) Human macrophages and RAW264.7 cells were silenced as described in Materials and methods, using control (siRNACtrl.) and lipin-2–specific siRNAs (siRNA*Lpin2*). (right) *Lpin2* mRNA levels at the time of stimulation. (D) BMDMs supernatants were analyzed by immunoblot using specific antibodies against IL-1β. (right) Densitometric quantification of the bands. (E) IL-1β production was analyzed in BMDMs supernatants from WT, *Nlrp3*$^{-/-}$, *Asc*$^{-/-}$, and *Casp1*$^{-/-}$ animals treated with a control siRNA (siRNACtrl.) or siRNAs against *Lpin2* (siRNA*Lpin2*) for 2 d, and then stimulated as indicated. (right) Level of *Lpin2* mRNA after silencing. Data from A–C and E are shown as means ± SD and are representative of at least three independent experiments made in triplicate. Data from D are representative of at least three independent experiments. *, $P < 0.05$; **, $P < 0.01$; ***, $P < 0.001$, Student's *t* test.

ERK inhibition (PD98059) had a modest but significant effect on *Il1b* mRNA generated in BMDMs from *Lpin2*$^{-/-}$ animals, but not in WT animals (Fig. 2 F). As expected from the mRNA expression data, when cells were treated with p38 inhibitor before the priming step, IL-1β release was strongly inhibited in both cellular phenotypes, abrogating the overproduction observed in lipin-2–deficient cells. ERK and JNK inhibitors reduced the overproduction generated in BMDMs from *Lpin2*$^{-/-}$ animals under these conditions (Fig. 2 G).

Phosphorylation events occurring after TLR4 activation may also impact NLPR3 inflammasome proteins, favoring the second step of inflammasome activation (Hara et al., 2013). We performed experiments where inhibitors were added between the priming and the inflammasome activation step to ensure that the pro–IL-1β was not perturbed (Fig. 2 G). Using this strategy, we found that ERK and p38 inhibition affected IL-1β maturation in lipin-2–deficient cells, decreasing cytokine production to levels found in WT cells, whereas JNK inhibition reduced IL-1β maturation in both WT and lipin-2–deficient cells.

We also observed that *Nlrp3* mRNA and NLPR3 protein levels were increased in BMDMs from *Lpin2*$^{-/-}$ animals (Fig. 2, H and I). Collectively, these results show that signaling during inflammasome priming by LPS is reduced by lipin-2.

Lipin-2 controls caspase-1 activation

To investigate the role of lipin-2 in inflammasome activation, we took advantage of the fact that pro–IL-18 is also

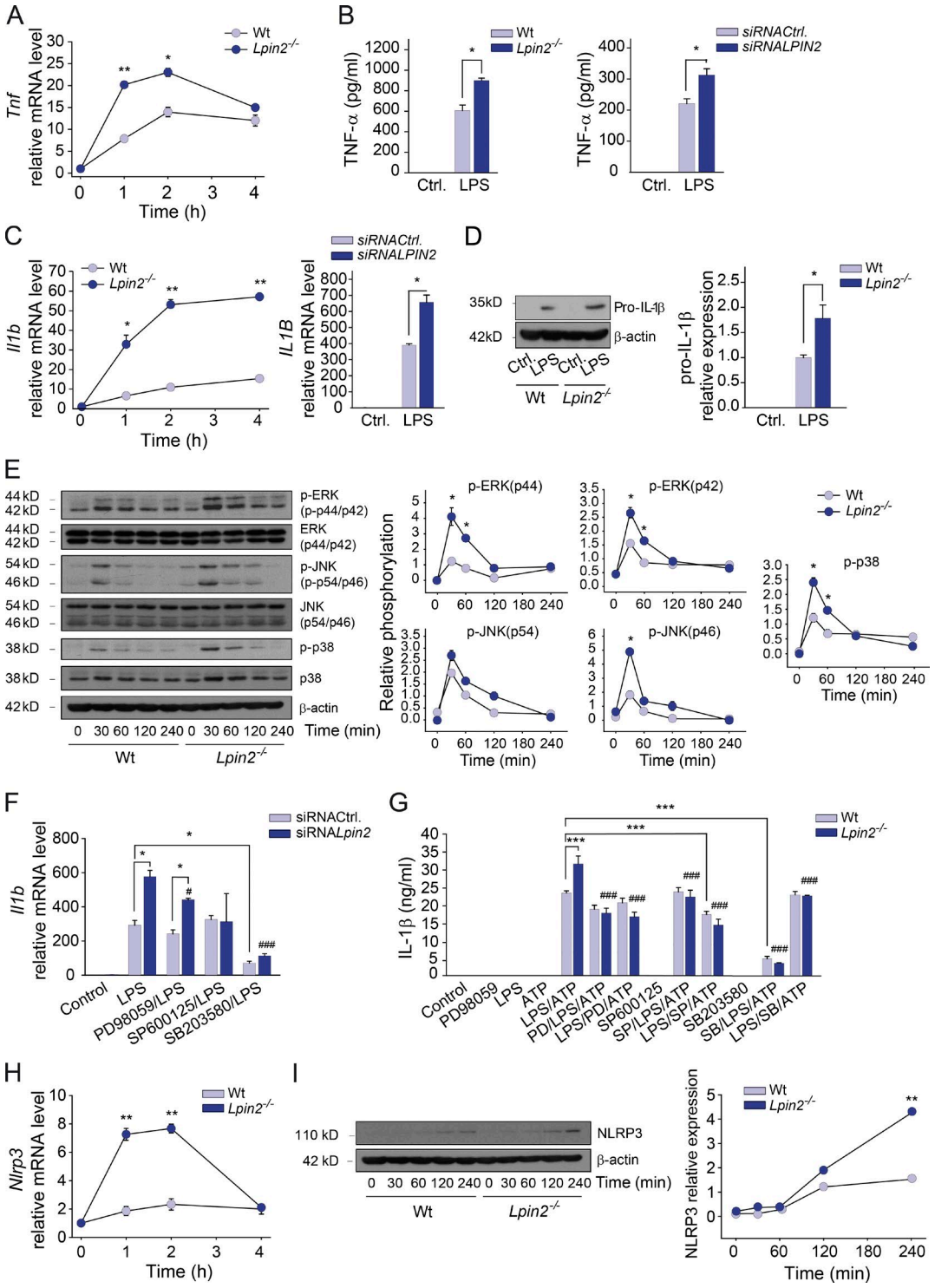

Figure 2. **The effect of lipin-2 on TLR4 signaling.** (A) WT and *Lpin2*$^{-/-}$ BMDMs were stimulated with 200 ng/ml LPS for the indicated periods of time, and then mRNA levels for *Tnf* were quantified by RT-qPCR. (B) Quantification of TNF present in cellular supernatants from WT and *Lpin2*$^{-/-}$ BMDMs (left) or silenced human macrophages (right) treated with 200 ng/ml LPS for 4 h. (C) Quantification of *Il1b* mRNA levels from WT and *Lpin2*$^{-/-}$ BMDMs (left), or silenced human macrophages (right) stimulated with LPS. (D) Analysis by Immunoblot of pro–IL-1β present in homogenates from BMDMs (left). (right) Relative expression levels of IL-1β against β-actin. (E) Analysis by immunoblot of MAPKs and their phosphorylated forms present in BMDMs activated as in A (left). (right) Relative quantification of phosphoproteins against total proteins. (F) Control (siRNACtrl.) and lipin-2–silenced (siRNALpin2) RAW264.7 cells were pretreated with 10 µM PD98059, SP600125, or SB203580 for 30 min, and then stimulated with 200 ng/ml LPS for 4 h. *Il1b* mRNA levels were

processed by activated caspase-1, but its expression is constitutive in cells (Gu et al., 1997). Our results showed that there was an increased production of IL-18 in *Lpin2*$^{-/-}$ BMDMs and lipin-2–deficient human macrophages compared with control cells, whereas the levels of mRNA for *Il18/IL18* did not change (Fig. 3, A and B). Of note, just ATP, without priming, was sufficient to produce mature IL-18, and the absence of lipin-2 further increased this production, indicating an overactivation of the inflammasome under these circumstances. We also found that BMDMs from *Lpin2*$^{-/-}$ animals had an increased release of mature caspase-1 after inflammasome activation compared with control cells (Fig. 3 C). Analysis of intracellular caspase-1 activity demonstrated that cells with reduced levels of lipin-2 were more prone to activate caspase-1 (Fig. 3 D). To further demonstrate that caspase-1 is responsible for IL-1β processing, the general inhibitor of caspases ZVAD as well as the specific inhibitor for caspase-1, YVAD, were used. Both of them effectively blocked the generation of IL-1β without affecting TNF generation in BMDMs from *Lpin2*$^{-/-}$ and WT animals, as well as in human macrophages (Fig. 3, E and F). As a consequence of caspase-1 activation, macrophages deficient in lipin-2 had increased pyroptosis levels after LPS plus ATP treatment, as shown by lactate dehydrogenase (LDH) release (Fig. 3 G). Analysis of propidium iodide (PI) incorporation confirmed that lipin-2–deficient cells were more permeable than WT cells after inflammasome activation (Fig. 3 H). Altogether, these experiments demonstrate that lipin-2 controls caspase-1 activation during classical inflammasome activation.

Lipin-2 inhibits inflammasome assembly

Oligomerization of ASC promoted by activation of the NLRP3 inflammasome is an upstream event that is responsible for recruitment and activation of caspase-1. We analyzed whether oligomerization of ASC was affected by lipin-2. Analysis of ASC oligomers performed by disuccinimidyl suberate cross-linking showed that BMDMs from *Lpin2*$^{-/-}$ mice had increased ASC oligomerization compared to control cells after inflammasome activation (Fig. 4 A). Also, examination of BMDMs by confocal microscopy showed an increased number of ASC specks (inflammasomes) and a tendency to produce bigger specks in cells from *Lpin2*$^{-/-}$ mice than cells from WT animals (Fig. 4, B–D). These results indicate that lipin-2 decreases ASC oligomerization and inflammasome assembly.

Lipin-2 regulates P2X7R pore formation

In the next series of experiments, we analyzed whether lipin-2 exerted any influence on the production of IL-1β by other NLRP3 activators in addition to ATP. Inflammasome was activated by nigericin, monosodium urate, and alum in primed macrophages (Fig. 5 A). Although there was a tendency for cells expressing low levels of lipin-2 to produce more IL-1β than control cells with the aforementioned NLRP3 activators, there was no significant difference. These results suggest that, of the NLRP3 activators tested, only the response to ATP was regulated by lipin-2. This finding led us to examine whether lipin-2 regulates the activity of $P2X_7R$. Whole-cell patch clamp experiments shown in Fig. 5 demonstrated that acute extracellular application of ATP activates inward (–120 mV) and outward (+100 mV) currents through the $P2X_7R$, whose amplitude is dramatically enhance in macrophages from *Lpin2*$^{-/-}$ mice compared with control cells. The reversion potential of the cells in those conditions was close to 0 mV, independent of lipin-2 expression levels (Fig. 5 B). When sodium in the standard extracellular solution was substituted by *N*-methyl-D-glucamine, an organic large monovalent cation, WT cells showed a significant reduction in inward currents after ATP treatment, with a reversion potential close to –50 mV. However, cells from *Lpin2*$^{-/-}$ mice underwent increased outward currents after ATP treatment. The reversion potential for these cells was –30 mV, i.e., very different from the membrane potential in resting conditions, which is close to –80 mV. By analyzing the mean current densities, we found that cells with reduced expression of lipin-2 have increased inward and outward currents during ATP stimulation (Fig. 5, C and D). These data suggest that ATP promotes the $P2X_7R$ opening to a dilated state that is larger when lipin-2 is absent.

The temporal course of $P2X_7R$ pore opening and closure was also studied. The data showed that although there was not a for the opening velocity of the pore (t_{on}) between cells with different levels of lipin-2, the $P2X_7R$ pore from *Lpin2*$^{-/-}$ cells experienced a delayed closure (higher t_{off}) compared with control cells (Fig. 5 E). Collectively, these results suggest that lipin-2 controls the amplitude of the $P2X_7R$ pore formed after challenging with ATP, and also the time the pore is open.

Lipin-2 controls intracellular K^+ levels and membrane permeability during $P2X_7R$ activation

Because the fall of intracellular K^+ levels is a mechanism for NLRP3 activation (Muñoz-Planillo et al., 2013) we

quantified by RT-qPCR. (G) WT and *Lpin2*$^{-/-}$ BMDMs were treated with inhibitors before or after stimulation with LPS. Stimulations were as indicated. IL-1β present in cellular supernatants is shown. (H) WT and *Lpin2*$^{-/-}$ BMDMs were stimulated with LPS as in A, and then Nlrp3 mRNA levels were quantified. (I) Analysis by immunoblot of NLRP3 present in cellular homogenates from BMDMs stimulated as in A (left). (right) Relative NLRP3 expression levels against β actin. β-Actin bands are the same as shown in E because the same blot was used. Data from A–C and F–H are shown as mean ± SD, and experiments shown are representative of at least three independent experiments made in triplicate. Data from D, E, and I are representative of at least three independent experiments. *, $P < 0.05$; **, $P < 0.01$; ***, $P < 0.001$, Student's *t* test. #, $P < 0.05$; ###, $P < 0.001$, versus siRNALpin2 + LPS cells (F), or *Lpin2*$^{-/-}$ + LPS/ATP cells (G) by Student's *t* test.

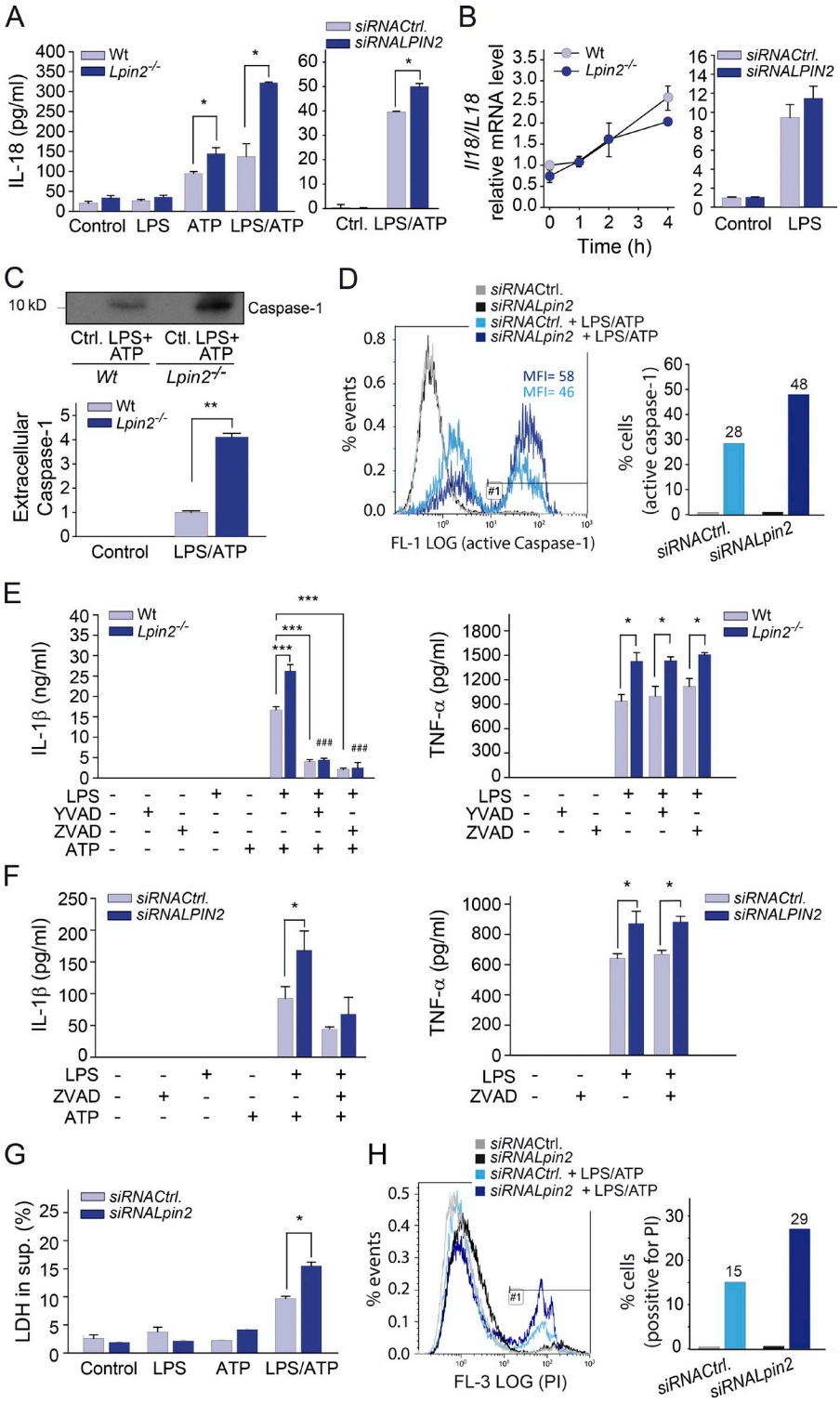

Figure 3. **The effect of lipin-2 on caspase-1 activation.** (A) WT and *Lpin2*$^{-/-}$ BMDMs (left) or silenced human macrophages (right) were stimulated with 200 ng/ml LPS for 4 h or the indicated periods of time, 2 mM ATP for 40 min, or both, as indicated. IL-18 present in cellular supernatants was quantified by specific ELISAs. (B) Cells as in A were stimulated with LPS and *Il18* mRNA levels were quantified by RT-qPCR. (C) Analysis by immunoblot of active caspase-1 present in supernatants from WT and *Lpin2*$^{-/-}$ BMDMs (top). (bottom) Densitometric quantification of the bands. (D) Analysis of intracellular active caspase by flow cytometry in RAW264.7 cells treated with control siRNA (siRNACtrl.) or siRNA against lipin-2 (siRNA*Lpin2*) and stimulated as in A. Median fluorescence intensities (MFI) are indicated (left). (right) Percentage of cells with active caspase-1. (E and F) WT and *Lpin2*$^{-/-}$ BMDMs (E) or silenced human macrophages (F) were pretreated with 10 µM YVAD or ZVAD for 30 min and then stimulated as in A. (G) IL-1β (left) and TNF (right) present in cellular supernatants were quantified by specific ELISAs. LDH release from RAW264.7 cells treated as in D. (H) Analysis by flow cytometry of RAW264.7 cells treated as in D and stained with propidium iodide (PI; left). (right) Percentage of cells positive for PI. Data from A, B, and E–G are shown as mean ± SD, and experiments shown are representative of at least three independent experiments made in triplicate. Data from C, D, and H are representative of at least three independent experiments. *, $P < 0.05$; **, $P < 0.01$; ***, $P < 0.001$, Student's *t* test. (E) ###, $P < 0.001$, versus *Lpin2*$^{-/-}$ + LPS/ATP cells by Student's *t* test.

studied whether lipin-2 influences intracellular K^+ levels in ATP-stimulated cells. The results showed that K^+ levels fell sharply after ATP treatment, nearing 10% of initial intracellular K^+ concentration in only 2 min (Fig. 6 A). Significant differences between WT and lipin-2–deficient cells were already found at this short time. After 4 min of treatment, intracellular K^+ concentrations started to recover, reaching a plateau at ∼15 min, with values of 27% for WT cells and 18% for lipin-2–deficient cells (Fig. 6 A). Thus, cells lacking lipin-2 maintained lower K^+ levels after ATP treatment than

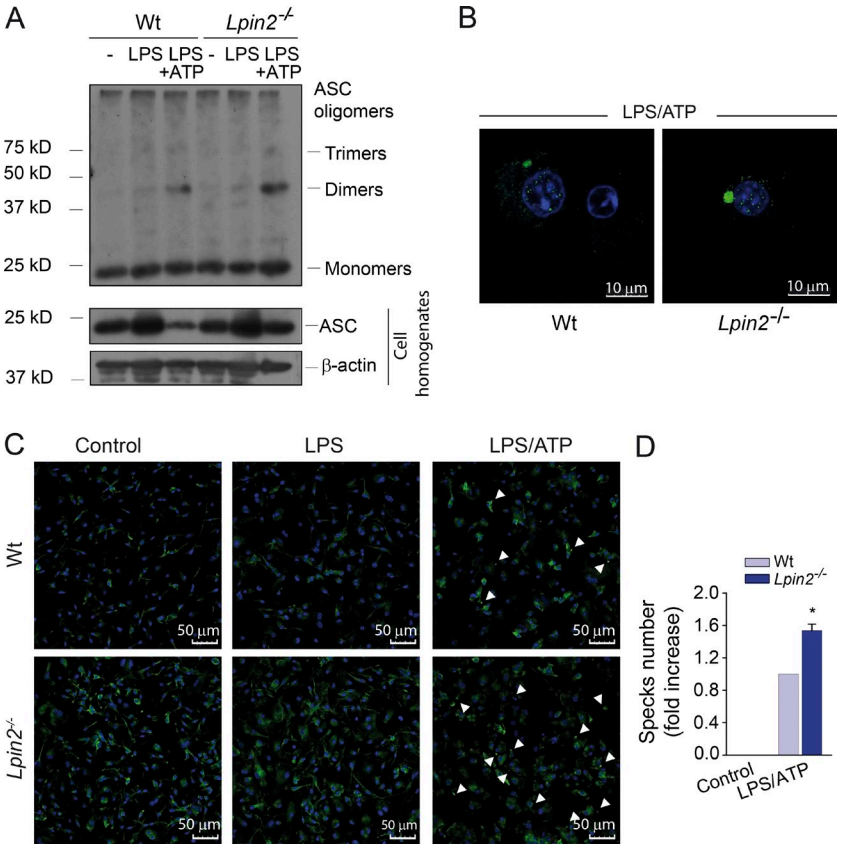

Figure 4. **The effect of lipin-2 on ASC oligomerization and inflammasome assembly.** BMDMs from WT and *Lpin2*$^{-/-}$ mice (A–D) were treated with 200 ng/ml LPS for 4 h, 2 mM ATP for 40 min, or both, as indicated. (A) Proteins from whole-cell lysates and purified cross-linked ASC oligomers were analyzed by immunoblot using specific antibodies against ASC or β-actin as a loading control. (B and C) Cells were stimulated as indicated and stained with specific antibodies against ASC and DAPI, as mentioned in the Materials and methods. Fluorescence was imaged by confocal microscopy. Bars: (B) 10 µm; (C) 50 µm. Arrowheads denote ASC specks. (D) Fold increase in ASC speck production from 700–1,400 cells is shown. Data from A–D are representative of at least three independent experiments. Data from D are shown as means ± SD *, $P < 0.05$, Student's *t* test.

WT cells. These results are fully consistent with the patch clamp experiments showing that $P2X_7R$ pore is larger and stays open for longer period of time in the absence of lipin-2, allowing a prolonged exit of K^+.

Experiments were then performed where extracellular K^+ concentrations were manipulated. At 45 mM extracellular K^+ (where the intracellular K^+ drop is prevented), the production of IL-1β was inhibited compared with 5 mM K^+ (the physiological extracellular concentration) in both lipin-2–deficient and control cells, and no significant differences could be found between them (Fig. 6 B). However, in the absence of extracellular K^+, which favors cellular exit of the cation, the production of IL-1β was higher in both WT and lipin-2–deficient cells than at physiological K^+ levels, but cells lacking lipin-2 were still able to produce more IL-1β than WT cells (Fig. 6 B). These experiments suggest again a key role for K^+ in the overactivation of the NLRP3 inflammasome in the absence of lipin-2.

Examination of $P2X_7R$ pore formation by analyzing the uptake of ethidium bromide in living cells by confocal microscopy showed that cells lacking lipin-2 displayed a higher and faster ethidium bromide uptake than WT cells (Fig. 6 C).

Increased membrane permeability generated by $P2X_7R$ activation at later stages can also be evaluated by the entrance of small proteins such as Annexin V, which binds to the phosphatidylserine molecules present in the internal leaflet of the cell membrane (Brennan and Cookson, 2000). Analysis of permeability to Annexin V showed that cells with reduced levels of lipin-2 displayed increased Annexin V binding to membranes, which was very evident after 50 min of ATP treatment (Fig. 6 D).

Altogether, these results indicate that lipin-2 reduces ATP-promoted K^+ efflux that is responsible for IL-1β production, as well as $P2X_7R$ pore formation, during classical inflammasome activation.

Lipin-2–deficient macrophages display low cholesterol levels that affect $P2X_7R$ activation

As a result of the role of lipin-2 in lipid metabolism, the assumption could be made that the effects of the enzyme on $P2X_7R$ would be related to changes in the composition or concentration of certain lipids. In this regard, cholesterol levels have been found to negatively regulate $P2X_7R$ activation (Michel and Fonfria, 2007; Robinson et al., 2014). We then analyzed cellular cholesterol levels in BMDMs from *Lpin2*$^{-/-}$ mice, and found that there was a significant reduction in its levels compared with WT cells (Fig. 7 A), especially in basal conditions and after stimulation with LPS. Differences in cholesterol levels were also found in lipin-2–silenced RAW264.7 cells under all conditions studied (Fig. 7 A). Experiments were conducted to reestablish cholesterol levels in cells deficient in lipin-2, and this was achieved by incubating

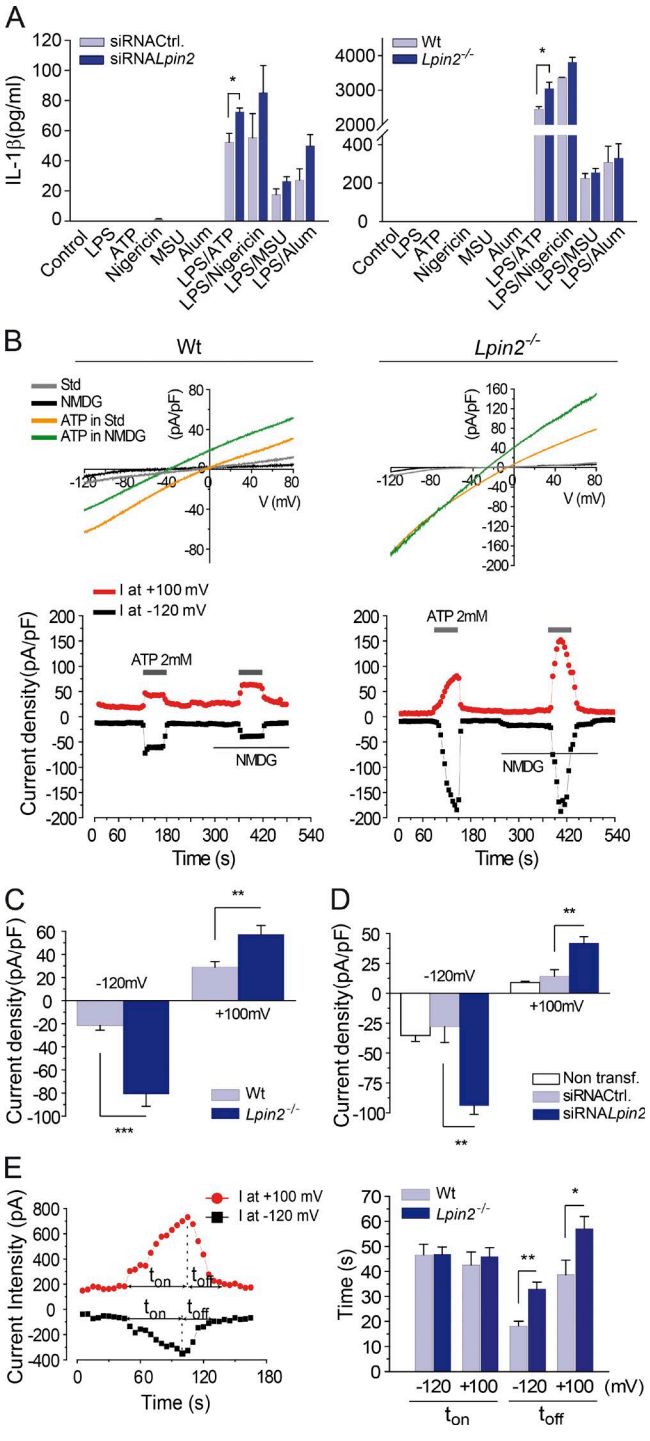

Figure 5. **The effect of Lipin-2 on cellular ionic currents generated by ATP.** RAW264.7 cells treated with control siRNA (siRNACtrl.), siRNA against lipin-2 (siRNA*Lpin2*; A, left), or BMDMs from WT and *Lpin2*$^{-/-}$ mice (A, right) were stimulated with 100 ng/ml LPS for 4 h, 2 mM ATP or 10 µM nigericin for 40 min, 200 µg/ml monosodium urate (MSU) or 150 µg/ml alum for 6 h, or LPS for 4 h, followed by ATP or nigericin for 40 min, MSU, or alum for 6 h, as indicated. IL-1β present in cellular supernatants was analyzed by specific ELISA (A). (B) Representative traces obtained with whole-cell recordings using a 1-s ramp protocol in peritoneal macrophages from WT and *Lpin2*$^{-/-}$ animals stimulated with 2 mM ATP in control solution (140 mM NaCl) or in a solution where NaCl has been substituted for 140 mM *N*-methyl-D-glucamine (NMDG), as indicated. (top) Current density versus voltage plots; (bottom) time course of the current density at −120 and +100 mV. (C) Mean current density from 25–39 macrophages analyzed is shown. RAW264.7 cells were also evaluated as in B and mean current density from 18 cells is shown (D). Time course of the current amplitude obtained at −120 mV and +100 mV in a peritoneal macrophage from WT mice upon exposure to 2 mM ATP during the indicated time, to illustrate the calculations of t_{on} (time from opening to maximal stimulation) and t_{off} (time from maximal opening to closure; E, left). (right) Mean t_{on} and t_{off} for −120 mV and +100 mV from WT and *Lpin2*$^{-/-}$ mice peritoneal macrophages (14–40 cells) stimulated with 2 mM ATP (E). Data from A are shown as mean ± SD, and experiments shown are representative of at least three independent ones made in triplicate. *, P < 0.05, Student's *t* test. Dada from C, D, and E, are shown as means ± SEM *, P < 0.05; **, P < 0.01; ***, P < 0.001, one-way ANOVA, followed by Tukey's test.

the cells with 100 µg/ml cholesterol loaded in methyl-β-cyclodextrin (MCD), to make it water soluble (Robinson et al., 2014). This treatment completely restored cholesterol levels in lipin-2–deficient cells (Fig. 7 B). These conditions were then used to study whole-cell currents mediated by the $P2X_7R$. We observed that pretreatment of cells with cholesterol profoundly reduced inward and outward currents generated by ATP treatment in macrophages from *Lpin2*$^{-/-}$ mice, producing no significant changes in WT cells (Fig. 7 C). Accordingly, mean current density analyses revealed that elevated inward and outward currents generated in lipin-2–deficient cells were reduced in those cells when cholesterol levels were restored, the effect being especially observable for outward currents (Fig. 7 D). Analyses of the temporal behavior of $P2X_7R$ showed that cholesterol treatment reduced the time needed for $P2X_7R$ to close (t_{off}) in macrophages from *Lpin2*$^{-/-}$ mice and again, the effect was especially relevant for the outward currents (Fig. 7 E). There were no effects of cholesterol on t_{off} for WT cells under these conditions. Overall these results are consistent with lipin-2 controlling the levels of cholesterol in macrophages, which in turn regulates $P2X_7R$ behavior, reducing current density through the channel by decreasing the opening of the pore and accelerating its rate of closure.

Cholesterol treatment reverses inflammasome overactivation in lipin-2–deficient cells

To assess whether restoration of cholesterol levels could affect the overactivation of the inflammasome in cells deficient in lipin-2, we evaluated $P2X_7R$ downstream events during inflammasome activation, i.e., ASC speck assembling, caspase-1 activation, and IL-1β production. For these experiments, cholesterol treatment was always performed 30 min before ATP treatment to evaluate only the effects on the second signal of inflammasome activation. Under these conditions, cholesterol loading reduced ASC oligomers present in BMDMs from *Lpin2*$^{-/-}$ mice to levels present in WT cells after inflammasome activation (Fig. 8 A).

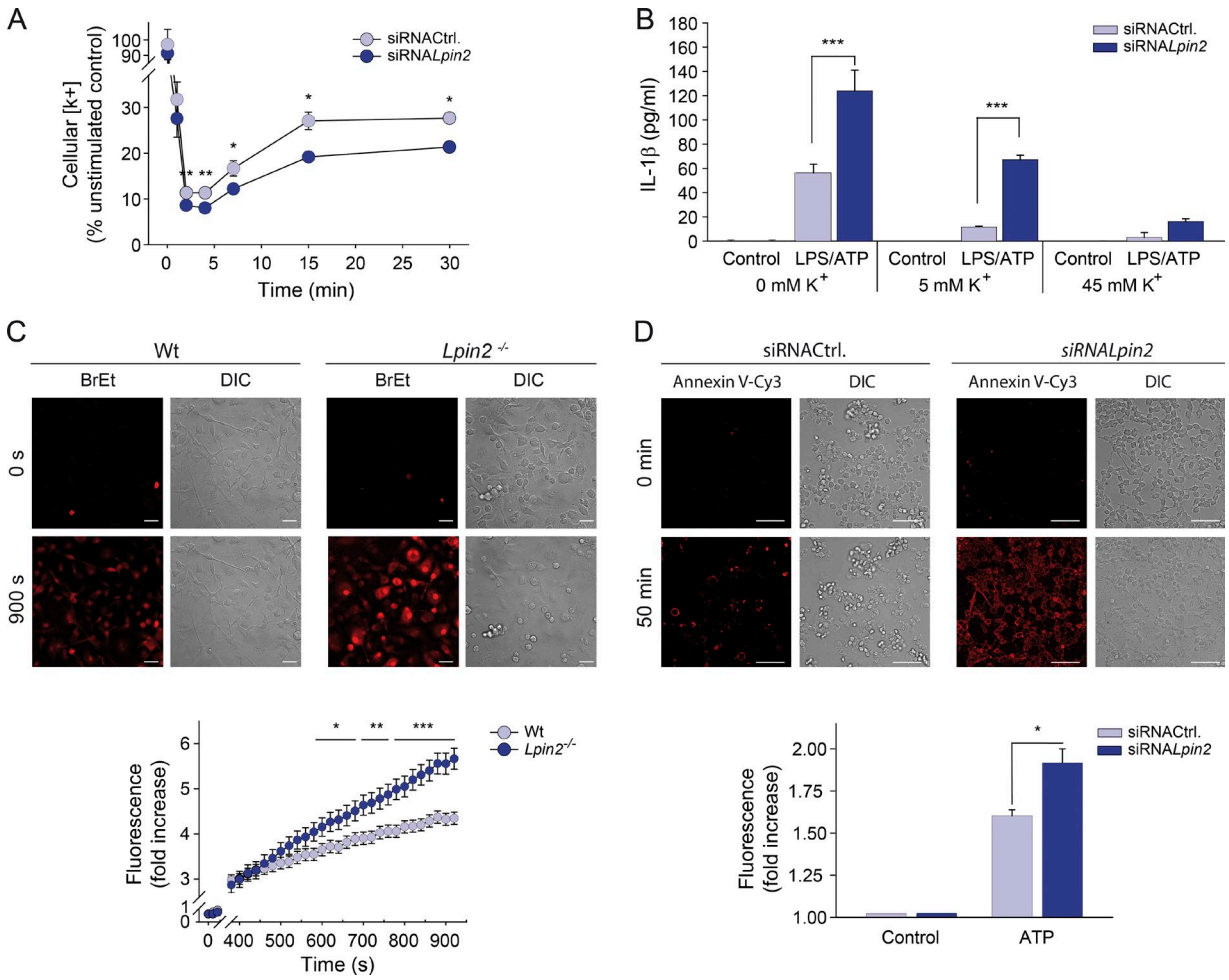

Figure 6. **Effect of lipin-2 on ATP-induced changes in K^+ cellular levels and cell permeability.** (A) Control (siRNACtrl.) and lipin-2–silenced (siRNA*Lpin2*) RAW264.7 cells were stimulated with 2 mM ATP for the indicated periods of time, and intracellular concentration of K^+ was analyzed using an inductively coupled plasma/optical emission spectrometer. (B) RAW264.7 cells were stimulated with 200 ng/ml LPS for 4 h, and then 2 mM ATP for 40 min, as indicated, in the presence of 0, 5, or 45 mM K^+. IL-1β present in cellular supernatants was analyzed by specific ELISAS. (C) BMDMs from WT and *Lpin2*$^{-/-}$ mice were pretreated with 20 µM ethidium bromide (BrEt) for 5 min, and then stimulated with 2 mM ATP. Ethidium cellular uptake was monitored by confocal microscopy. (top) Cell fluorescence; (bottom) fluorescence fold increase over time. Bar, 25 µm. (D) Control (siRNACtrl.) and lipin-2–silenced (siRNA*Lpin2*) RAW264.7 cells were stimulated with 2 mM ATP for 50 min in the presence of Annexin-V-Cy3, and fluorescence analyzed in a confocal microscope (top). (bottom) Fluorescence fold increase over unstimulated cells. Bar, 50 µm. Data from A and B are shown as mean ± SD, and experiments shown are representative of at least three independent experiments made in triplicates. Data from C (>100 cells) and D (>300 cells) are shown as means ± SEM, and experiments shown are representative of at least three independent ones. *, $P < 0.05$; **, $P < 0.01$; ***, $P < 0.001$, by Student's *t* test.

When caspase-1 activation was analyzed by flow cytometry, it was also found that cholesterol treatment reduced both the amount of active caspase-1 per cell (MIF) and the percentage of cells that have active caspase-1 in lipin-2–deficient cells, with no significant changes in control cells (Fig. 8 B). Finally, IL-1β production was reduced by cholesterol treatment in cells deficient in lipin-2 without significant changes in control cells (Fig. 8 C). Collectively, these results demonstrate that restoration of cholesterol levels during the second signal of inflammasome activation reduces inflammasome assembly, caspase-1 activation, and IL-1β production in cells deficient in lipin-2.

Lipin-2 restrains inflammasome activation in vivo in mice

To assess whether the observed effects of lipin-2 on inflammasome activation in vitro could be translated to in vivo animal models of inflammasome activation, we evaluated IL-1β production in animals after 3 h of intraperitoneal injection of 10 mg/kg LPS. Consistent with our previous results, *Lpin2*$^{-/-}$ mice had exacerbated responses to LPS, producing higher amounts of IL-1β (Fig. 9 A). In addition, we also observed enhanced production of IL-18 (confirming inflammasome activation) and TNF (confirming TLR4 enhanced activation), although in the latter case differences were less pronounced (Fig. 9 A). Analysis of tissues that undergo a strong inflamma-

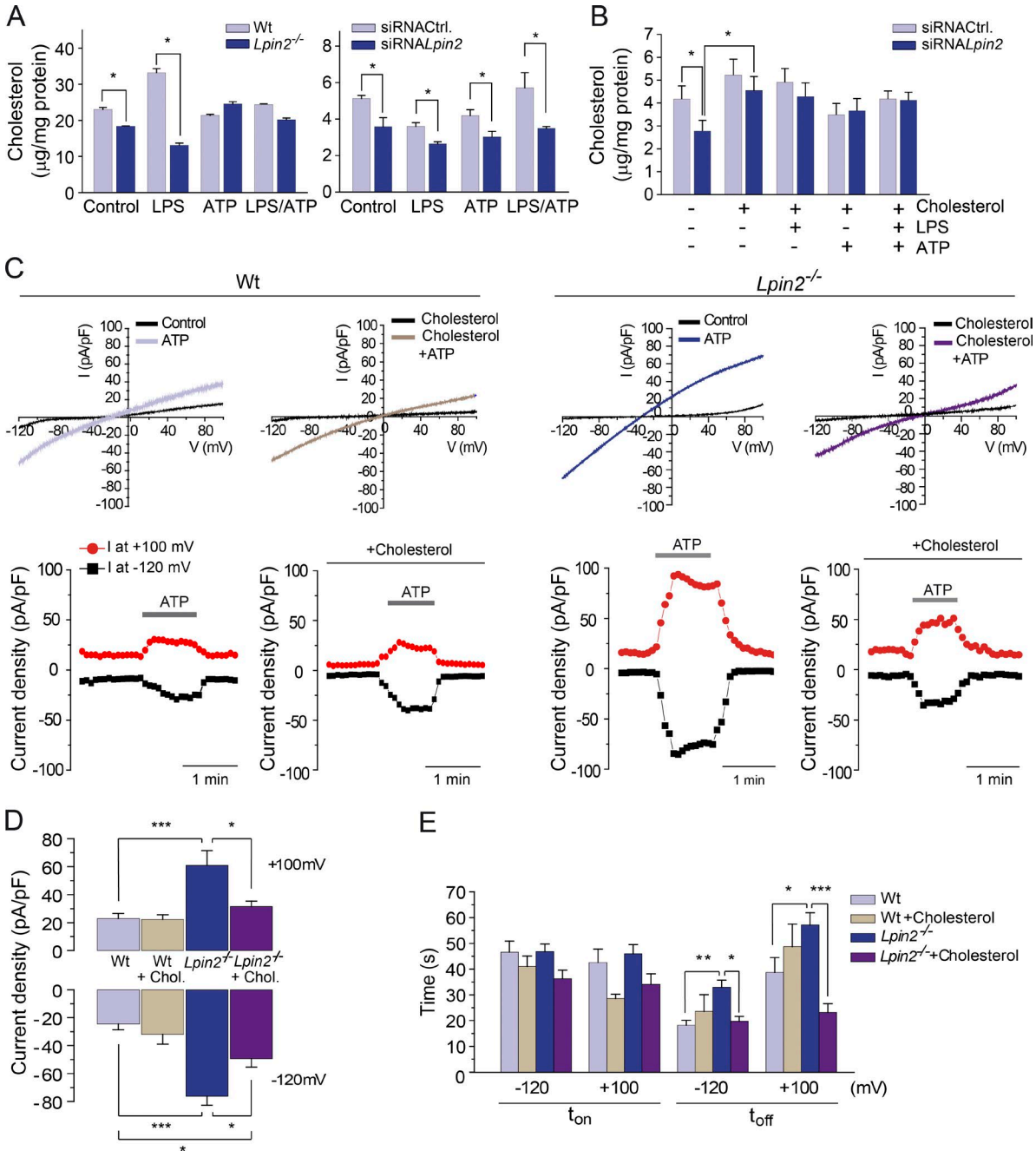

Figure 7. **Impact of lipin-2 on cellular cholesterol levels, and restoration of P2X$_7$R functionality by cholesterol in the absence of lipin-2.** (A) BMDMs from WT and *Lpin2*$^{-/-}$ mice (left), or control (siRNACtrl.) and lipin-2–silenced (siRNA*Lpin2*) RAW264.7 cells (right) were treated with 200 ng/ml LPS for 4 h, 2 mM ATP for 40 min, or both, as indicated. (B) Total cellular cholesterol levels were analyzed as described in Materials and methods. RAW264.7 cells preincubated with 100 µg/ml cholesterol (cholesterol/MCD) for 30 min were treated as in A, and total cellular cholesterol levels were measured. (C) Example traces of whole-cell ionic currents analyzed by patch-clamp in peritoneal macrophages from WT and *Lpin2*$^{-/-}$ animals stimulated with 2 mM ATP in the absence or presence of 100 µg/ml cholesterol (cholesterol/MCD) as indicated. (top) Current density against voltage; (bottom) current densities at −120 and +100 mV. (D) Mean current density from 15–18 cells analyzed. (E) The mean t_{on} and t_{off} at −120 and +100 mV from WT and *Lpin2*$^{-/-}$ mice peritoneal macrophages stimulated with 2 mM ATP in the presence or absence of 100 µg/ml cholesterol (cholesterol/MCD). Data from A and B are shown as mean ± SD, and experiments shown are representative of at least three independent experiments made in triplicate. Data from D and E are shown as means ± SEM *, P < 0.05; **, P < 0.01; ***, P < 0.001, Student's *t* test (A and B) or by one-way ANOVA followed by Tukey's test (D and E).

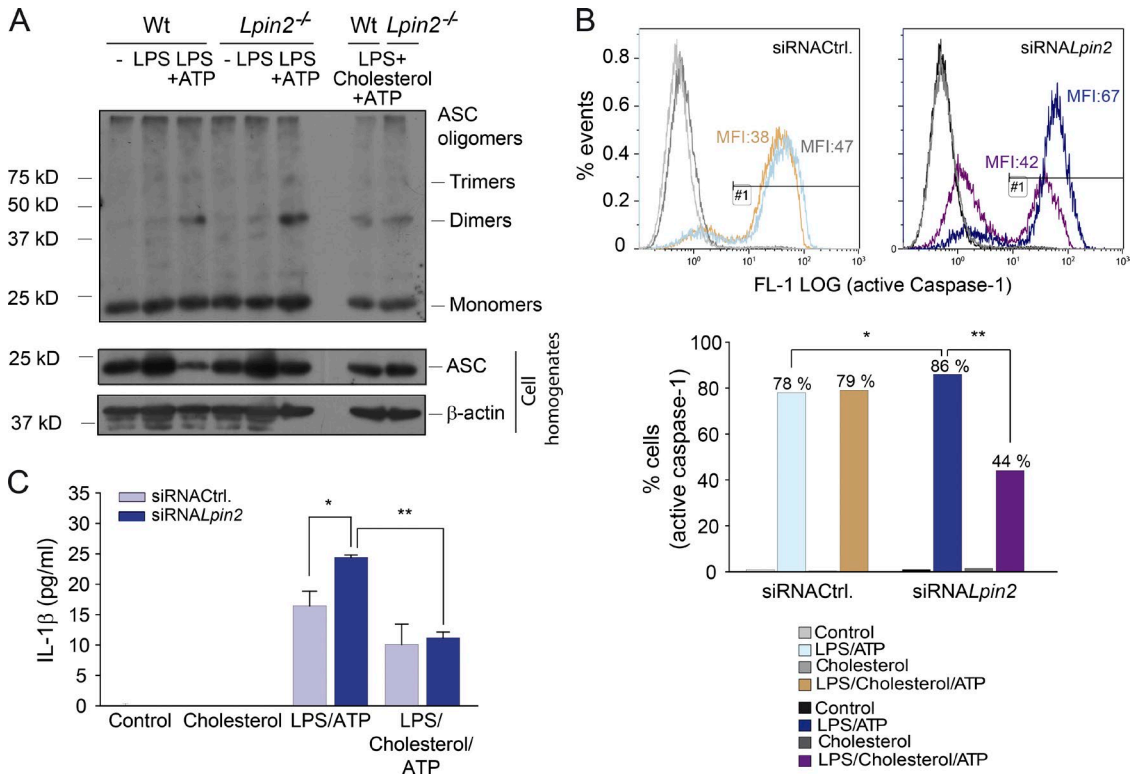

Figure 8. **Cholesterol effect on ASC oligomerization, capase-1 activation, and IL-1β production in the absence of lipin-2.** (A) BMDMs from WT and *Lpin2*$^{-/-}$ mice were treated with 200 ng/ml LPS for 4 h, 2 mM ATP, or both, as indicated. Some samples were preincubated with 100 µg/ml cholesterol 30 min before ATP treatment, as indicated. Proteins from whole-cell lysates and purified cross-linked ASC oligomers were analyzed by immunoblot using specific antibodies against ASC or β-actin, as a loading control. (B) Control (siRNACtrl.) or lipin-2–silenced (siRNA*Lpin2*) RAW264.7 cells were treated with 200 ng/ml LPS for 4 h and then 2 mM ATP for 40 min, as indicated. Some samples were preincubated with 100 µg/ml cholesterol (cholesterol/MCD) 30 min before ATP treatment, as indicated. Intracellular active caspase was analyzed by flow cytometry as specified in Materials and methods. Median fluorescence intensities (MFI) are indicated. (bottom) Percentage of cells with active caspase-1. (C) RAW264.7 cells were treated as in B and presence of IL-1β in cellular supernatants was quantified by specific ELISA in triplicate samples. Data are shown as means ± SD, and experiments shown are representative of at least three independent experiments. *, $P < 0.05$; **, $P < 0.01$, by Student's *t* test.

tory response during LPS treatment demonstrated that the liver of animals deficient in lipin-2 have stronger responses to treatment with the endotoxin, producing higher levels of mRNA for *Il1b*, *Il6*, *Tnf*, *Il12b*, *Nos2*, and *Il1r* (Fig. 9 B). In parallel, there was a higher production of *Il1b* and *Tnf* in the spleen (Fig. 9 C). It should also be noted that mRNA expression of antiinflammatory cytokines like *Il10* was significantly reduced in spleens of *Lpin2*$^{-/-}$ mice (Fig. 9 C). There were increased *Nlrp3* mRNA levels in livers and spleens of animals deficient in lipin-2 after LPS treatment. Collectively, these results confirm the inhibitory role of lipin-2 during inflammasome activation in vivo.

DISCUSSION

Inflammasome activation is a complex process where many different pathways converge, but the contribution of lipid-related enzymes has been scarcely investigated to date. Here, we describe that lipin-2, a phosphatidic acid phosphohydrolase, plays a significant regulatory role, by modulating the extent of inflammasome activation via different mechanisms (Fig. 9 D). In the first place, lipin-2 reduces MAPKs activation during the priming phase, thus diminishing the levels of pro–IL-1β. Second, lipin-2 facilitates an appropriate lipid environment for $P2X_7R$, which regulates the amplitude of the pore formed after activation and the open to close transitions. As a consequence of this, ion currents are lower, especially K^+ currents, which negatively impact on NLRP3 inflammasome activation, ASC oligomerization, pro–caspase-1 processing and IL-1β and IL-18 maturation. These findings are of pathophysiologically relevance, as mutations in the *LPIN2* gene produce an autoinflammatory condition, and provide a mechanism by which a lipid-related enzyme controls inflammasome activation in murine and human macrophages. Thus, the results may help formulate new avenues for the treatment of patients with Majeed syndrome, whose symptoms are treated at this moment with expensive biological therapies using antibodies against IL-1β or recombinant IL-1 receptor antagonists (Herlin et al., 2013).

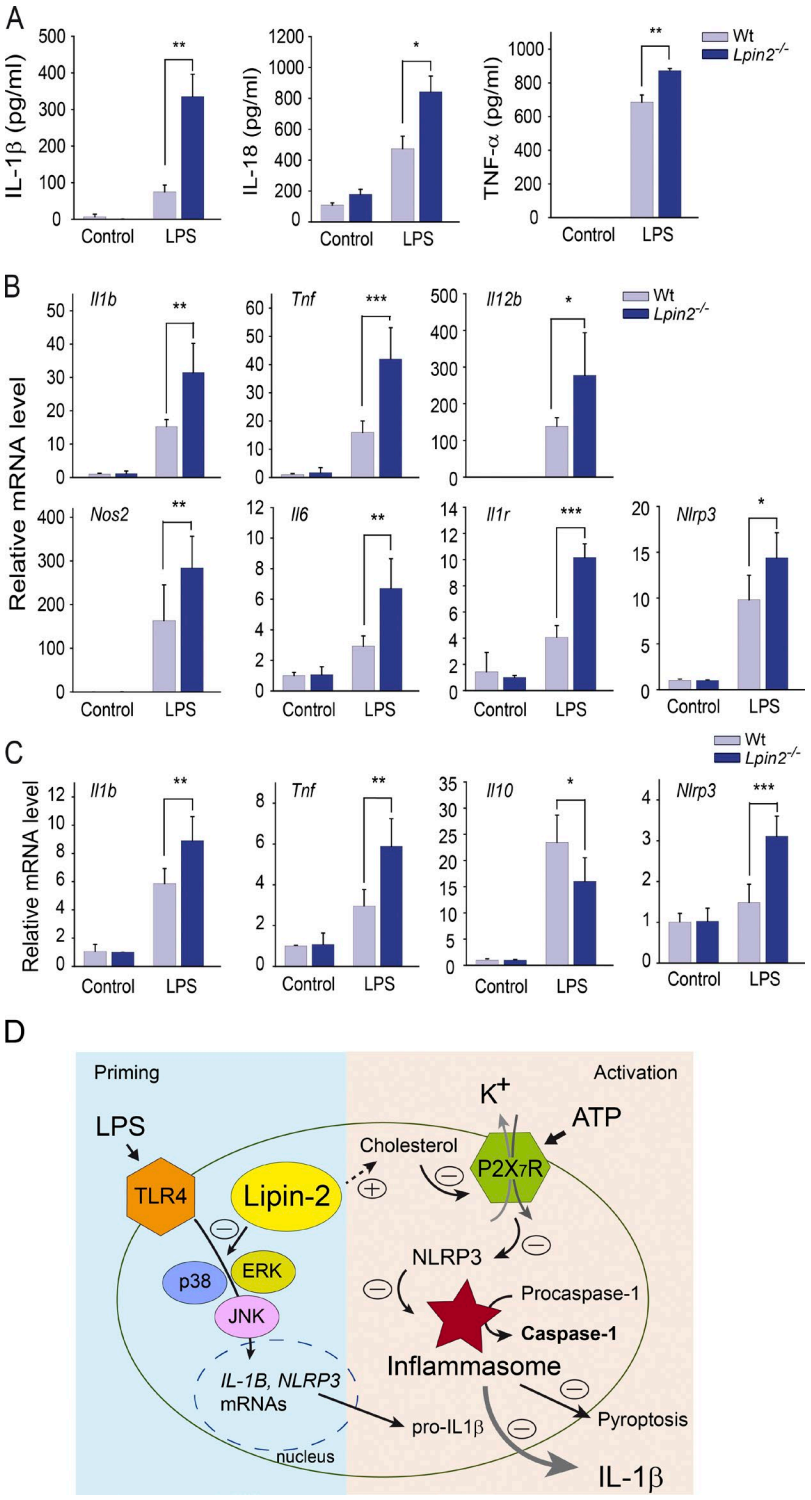

Figure 9. **The effect of lipin-2 in the response to LPS in mice.** (A) WT and *Lpin2*$^{-/-}$ mice (n = 5) were intraperitoneally injected with 10 mg/kg of LPS or PBS. 3 h later, indicated cytokines were quantified in serum using specific ELISA. Expression levels of the indicated genes were analyzed in liver (B) or spleen (C) by RT-qPCR. (D) Proposed scheme depicting lipin-2 effects on priming and activation of the inflammasome. Data are shown as means ± SD, and experiments shown are representative of at least two independent ones analyzed in triplicates. *, P < 0.05; **, P < 0.01; ***, P < 0.001, by Student's t test.

Lipin-2 restricts overphosphorylation of ERK, p38, and JNK, with different consequences for IL-1β synthesis. The effect of p38 on *Il1b* mRNA levels was previously described in cell lines (Baldassare et al., 1999), and our current results confirm this to happen in primary cells as well. We have found that the control that lipin-2 exerts over p38 is also key during IL-1β maturation. Overall, p38 inhibition results in >85% reduction in IL1-β production, which provides a very interesting possibility to consider as an alternative strategy for the treatment of patients with Majeed syndrome.

However, p38 might still be a very upstream target in the signaling cascade that culminates in the generation of *Il1b* mRNA, in which case it would be important to elucidate the downstream transcription factors that are affected by the kinase, especially in the absence of lipin-2. In this regard, C/EBPβ has been shown to be responsible of IL-1β up-regulation (Baldassare et al., 1999; Basak et al., 2005). On the other hand, ERK and JNK seem to specifically control IL-1β maturation in cells lacking lipin-2, although ERK may also affect mRNA levels for the cytokine in those circumstances. In this context, a key role has been described for JNK that, by phosphorylating ASC in Tyr144, promotes ASC specks assembling and caspase-1 activation (Hara et al., 2013). No evidence exists to date that ERK could also have a role on inflammasome assembly/activation.

A recent work on mutational analysis of $P2x_7R$ suggests the involvement of multiple cholesterol recognition amino acid consensus motifs in the N and proximal C-terminal region of the receptor that could be related to the cholesterol sensitivity of channel gating (Robinson et al., 2014). However, it is also possible that reduced cholesterol levels increases membrane fluidity and/or arrangement of other lipids around the receptor, promoting a state of pore dilation. The fact that cholesterol levels are altered by lipin-2 and that the $P2X_7R$ functionality is also modified by lipin-2 lead us to speculate about the possible involvement of this lipid in the regulation that the enzyme exerts on $P2X_7R$ responses. In this regard, our results raise intriguing questions as to how lipin-2 may regulate cholesterol levels in cells. Other lipins, such as lipin-1, have previously been described to regulate SREBP nuclear protein abundance and up-regulation of cholesterol and lipid biosynthetic enzymes (Peterson et al., 2011). The effect takes place by inhibiting mTORC1 activity and dephosphorylation of lipin-1, but the mechanism by which lipin-1 directly inhibits SREBP nuclear presence has not yet been elucidated (Peterson et al., 2011). It is possible that lipin-2 may also regulate SREBP activity/localization or any other important step that determines cellular cholesterol homeostasis: influx, synthesis, esterification, or efflux. Ongoing work in our laboratory using lipin-2–overexpressing cells (Valdearcos et al., 2012) suggests that cellular levels of cholesterol are elevated, and we are trying to define which of the aforementioned events are affected.

In addition to NLRP3, the possibility exists that other IL-1β–producing inflammasomes may also be affected by lipin-2 deficiency. Our preliminary observations suggest that the NLRC4 could be one of these (unpublished data). Recently, the pyrin inflammasome has been found to be activated after inactivation of RhoA GTPases by bacterial toxins (Xu et al., 2014; Park et al., 2016). RhoA needs to be geranylgeranylated for membrane targeting and full activity (Hori et al., 1991). Geranylgeranyl pyrophosphate, a metabolite of the intermediate of the cholesterol synthesis pathway farnesyl pyrophosphate, is the substrate for protein geranylgeranylation (Lutz et al., 1992). Because the results of our study show that lipin-2–deficient cells exhibit decreased cholesterol content, it is tempting to speculate that the production of geranylgeranyl pyrophosphate could be decreased as well, this leading to deficient RhoA geranylgeranylation and activation. In such scenario, the pyrin inflammasome activation would be enhanced. Studies are currently in progress to examine this attractive hypothesis.

The increased sensitivity of $Lpin2^{-/-}$ mice to inflammation induced by LPS emphasizes the role of lipin-2 as a critical regulator of inflammation in vivo, and recapitulates the findings in vitro. Because significant effects on inflammasome activation and systemic inflammation were already observed at 3 h LPS, we did not conduct measurements at longer times. We do not rule out that, with longer times of LPS exposure, bone inflammation and damage may develop, as reported by others (Sakuma et al., 2000; Ochi et al., 2010). In these models, significant bone damage takes 2–10 d of LPS treatment to occur. The process is slow, likely because new osteoclasts need to differentiate from their precursors in the bone marrow (Udagawa et al., 1990). Similar to previous observations, we have not found any particular autoinflammatory phenotype in otherwise untreated animals (Dwyer et al., 2012). This behavior further strengthens the hypothesis that the way animals are stocked may preclude their exposure to ambient contaminants or microorganisms that could possibly trigger those symptoms (Dwyer et al., 2012). Nevertheless, based on our results, the differences between patients and mutant mice could also be related to differences in the human versus the mice $P2X_7Rs$. The human receptor seems to be much more sensitive to cholesterol level changes than the murine receptor (Robinson et al., 2014), which suggests that in humans small modifications in the concentration of cholesterol could exacerbate $P2X_7R$ function and inflammasome activation when the proper circumstances are present.

Studies in humans and murine models have revealed that $P2X_7R$ is involved in many immunoinflammatory, neurological, and musculoskeletal disorders (Bartlett et al., 2014). Because diminished lipin-2 levels appears to increase $P2X_7R$ activity, the possibility exists that Majeed syndrome patients would be more susceptible to the development of other disorders different from autoinflammation, which are related to dysregulated $P2X_7R$ activity.

Overall our studies reveal the importance of lipin-2 in the control of TLR4 signaling, and $P2X_7R$ activation and sensitization, that finally culminate in a restricted activation of NLRP3 inflammasome. The results presented here may provide clues to better understand the molecular features that characterize the high IL-1β production found in patients with Majeed syndrome, and may open avenues for the development of new treatments that help to control or cure this condition.

MATERIALS AND METHODS

Reagents

LPS from *Escherichia coli* 0111:B4, the antibody against β-actin (A5441), SP600125, PD98059, and cholesterol-water

soluble were obtained from Sigma-Aldrich. Antibodies against phospho-p38 MAPK (Thr180/Tyr182; 4511), p38 MAPK (9212), phospho-p44/42 MAPK (Thr202/Tyr204; 9101), p44/42 MAPK (4695), phospho-SAPK/JNK (Thr183/Tyr185; 4668), SAPK/JNK (9252), and IL-1β (12242) were purchased from Cell Signaling Technology. Antibodies against ASC (22514), and active caspase-1 (sc-514 and 515) were obtained from Santa Cruz Biotechnology, Inc. Specific ON-Target plus siRNAs against murine mRNAs were obtained from Thermo Fisher Scientific. Silencer Select siRNAs specific to decrease the expression of human *LPIN2* mRNA and negative controls were purchased from Ambion. Nigericine, the specific caspase-1 inhibitor Ac-YVAD-AOM, and SB203582 were purchased from EMD Millipore, and monosodium urate and alum were obtained from InvivoGen. The general caspase inhibitor Z-VAD-FMK was from APExBIO. The rest of the reagents were purchased from Sigma-Aldrich.

Animals

The C57BL/6N*Lpin2*$^{tm1b(KOMP)Wtsi}$/Tcp mouse line deficient in lipin-2 (*Lpin2*$^{-/-}$) was made by the NorCOMM2 Project from KOMP ES cells and provided by the Canadian Mouse Mutant Repository at the Toronto Centre for Phenogenomics (Toronto, Canada). Untreated animals present increased red cell distribution width and thrombocytosis, and do not exhibit signs of osteomyelitis or systemic inflammation. This phenotype is concordant with that previously described by Dwyer et al. (2012). Animals were bred as heterozygotes at the Service of Animal Research and Welfare (University of Valladolid, Valladolid, Spain) and maintained in filter-top cages and were provided with water and food ad libitum (Global diet 2014; Harlan). 8–12-wk-old sex-matched animals were used for experimentation and WT littermates were used as controls. For LPS treatment, animals were injected i.p. with 10 mg/kg LPS in PBS. After 3 h, blood was collected from the facial vein and animals were euthanized for spleen and liver collection. All the protocols and procedures were approved by the Institutional Animal Care and Usage Committee and are in accordance with the Spanish and European Union guidelines for the use of experimental animals.

Cells

Peritoneal macrophages were obtained, as previously described (Meana et al., 2014), by flushing the peritoneal cavity with 5 ml ice-cold PBS. Cells were then centrifuged at 300 *g* for 10 min and allowed to adhere to glass coverslips overnight. Nonadherent cells were washed away with PBS and attached cells were maintained in culture until use.

BMDMs were differentiated from precursors obtained from WT, *Lpin2*$^{-/-}$, *Asc*$^{-/-}$ (Mariathasan et al., 2004), *Casp1/11*$^{-/-}$ (Kuida et al., 1995), and *Nlrp3*$^{-/-}$ (Martinon et al., 2006) mice femurs aseptically dislocated from the hind legs of the mice as previously described (Meana et al., 2014). In brief, isolated cells were cultured for 7 d in RPMI 1640 with 10% FBS, 100 U/ml penicillin, and 100 µg/ml streptomycin, supplemented with 20% conditioned medium from L929 cells.

Human macrophages were differentiated from blood monocytes obtained from healthy donors as previously described (Valdearcos et al., 2011) and lipin-2 levels were reduced using specific siRNAs from Ambion (sense sequence, 5′-GAAGUUGGGUGAUAACGGATT-3′, and antisense sequence 5′-UCCGUUAUCACCCAACUUCAT-3′) introduced in 10–14-d differentiated cells by Nucleofection (Amaxa Biosystems) as recommended by the manufacturers (Y-010 program). Usually, as much as 85–90% reduction of *Lpin2* mRNA was achieved by this methodology after 2 d of macrophage transfection.

RAW264.7 cells were cultured in DMEM supplemented with 10% FBS, 2 mM L-glutamine, 100 U/ml penicillin, and 100 µg/ml streptomycin. Lipin-2 levels were reduced using 20 nM ON-TARGET plus SMART pool siRNAs (Thermo Fisher Scientific) introduced with Lipofectamine RNAiMAX (Thermo Fisher Scientific) as specified by the manufacturer. After 2 d of transfection, *Lpin2* mRNA levels decreased 60–80% (Valdearcos et al., 2012).

ELISA assays

Cell supernatants were clarified by centrifugation at 15,000 *g* for 10 min, and 100 µl were used for determinations. Measurements to quantify TNF, IL1-β, and IL-18 were performed using specific ELISA assays as detailed in manufacturer's instructions (eBioscience).

Immunoblots

Cells were lysed with the buffer 20 mM Tris, pH 7.4, 150 mM NaCl, 1 mM EDTA, 1 mM EGTA, 5 mM $Na_4P_2O_7$, 50 mM β-glycerophosphate, 270 mM sucrose, 0.1% 2-mercaptoethanol, 1% Triton X-100, 100 µM PMSF, 1 mM Na_3VO_4, 10 mM NaF, and a protease inhibitor cocktail (P-8340; Sigma-Aldrich). Homogenates were centrifuged at 15,000 *g* for 10 min, and 50–100 µg of supernatants protein were separated by standard SDS-PAGE and transferred to PVDF membranes. Blocking was performed with 5% defatted dry milk or 5% bovine serum albumin in PBS (pH 7.4) for 1 h at room temperature. In general, primary antibodies were used at 1:1,000 in PBS with 0.5% defatted dry milk and 0.1% Tween-20. The exceptions were anti-caspase-1, ASC, and β-actin that were used at 1:250, 1:500, and 1:20,000, respectively. After extensive washes, secondary antibodies HRP linked were used at 1:5,000 dilution. Specific proteins were visualized using ECL chemiluminescent substrate (GE Healthcare).

Proteins from cellular supernatants were clarified of cells by centrifugation at 300 *g* for 8 min at 4°C and were then concentrated by centrifugation at 15,000 *g* for 30 min at 4°C using a 10-kD centrifugal filter unit (EMD Millipore).

ASC oligomers

Analysis of ASC oligomers was done as previously described, with a few modifications (Chuang et al., 2013; Compan et

al., 2015). In brief, cells were lysed in the buffer 10 mM Tris-HCl, pH 7.5, 10 mM NaCl, 3 mM $MgCl_2$, 0.1 mM EGTA, 100 µM Na_3VO_4, 1 mM PMSF, and a protease inhibitor cocktail (P-8340; Sigma-Aldrich) passed 30 times through a 21-gauge syringe. Cell lysates were centrifuged at 5,200 *g* for 8 min at 4°C to discard nuclei. Supernatants were diluted with equal volumes of buffer 20 mM Hepes-KOH, pH 7.5, 5 mM $MgCl_2$, 0.5 mM EGTA, 0.1% CHAPS, and centrifuged at 4,000 *g* for 8 min at 4°C to obtain the ASC oligomers. The pellets were then resuspended in the mentioned CHAPS buffer with 2 mM disuccinimidyl suberate as a cross-linker. Reactions were incubated at room temperature for 30 min and centrifuged at 4,000 *g* for 10 min. Pelleted oligomers were analyzed by Immunoblot.

RT-qPCR

Total RNA was extracted using TRIzol reagent (Ambion). cDNA was obtained using RETROscript kit Reverse Transcription for RT-PCR (Thermo Fisher Scientific), following the manufacturer's instructions. Quantitative real time-PCR analysis was performed in a LightCycler 480 (Roche) using specific primers, 40 ng cDNA, and the KAPA SYBR Master mix for RT-qPCR (Roche). Relative mRNA expression was obtained using the $^{\Delta\Delta}$Ct method using *Cyclophilin*, *actin*, or *Gapdh* as reference genes (Livak and Schmittgen, 2001).

Primers used for murine genes were as follows: *Lpin2*, 5′-AGTTGACCCCATCACCGTAG-3′ and 5′-CCCAAAGCATCAGACTTGGT-3′; *Il1b*, 5′-GCAACTGTTCCTGAACTCAACT-3′ and 5′-TCTTTTGGGGTCCGTCAACT-3′; *Il18*, 5′-CAAACCTTCCAAATCACTTCCT-3′ and 5′-TCCTTGAAGTTGACGCAAGA-3′; *Nlrp3*, 5′-ATCAACAGGCGAGACCTCTG-3′ and 5′-GTCCTCCTGGCATACCATAG-3′; *Casp1*, 5′-CTTGGAGACATCCTGTCAGGG-3′ and 5′-AGTCACAAGACCAGGCATATTC-3′; *Il1r1*, 5′-GTGCTACTGGGGCTCATTTG-3′ and 5′-GGAGTAAGAGGACACTTGCG-3′; *Il6*, 5′-TAGTCCTTCCTACCCCAATTTCC-3′ and 5′-TTGGTCCTTAGCCACTCCTTC-3′; *Tnf*, 5′-ACGGCATGGATCTCAAAGAC-3′ and 5′-AGATAGCAAATCGGCTGACG-3′; *Il12b*, 5′-TGGTTTGCCATCGTTTTGCTG-3′ and 5′-ACAGGTGAGGTTCACTGTTTCT-3′; *Nos2*, 5′-CCAAGCCCTCACCTACTTCC-3′ and 5′-CTCTGAGGGCTGACACAAGG-3′; *Il10*, 5′-GCTCTTACTGACTGGCATGAG-3′ and 5′-CGCAGCTCTAGGAGCATGTG-3′; *Ppib* (Cyclofilin B), 5′-TGGAGAGCACCAAGACAGAC-3′ and 5′-TGCCGGAGTCGACAATGAT-3′; and *Gapdh*, 5′-AGGTCGGTGTGAACGGATTTG-3′ and 5′-TGTAGACCATGTAGTTGAGGTCA-3′. Primers used for human genes were as follows: *LPIN2*, 5′-CCTCTCCTCAGACCAGATCG-3′ and 5′-GGAGAATCTGTCCCAAAGCA-3′; *IL1B*, 5′-ATGATGGCTTATTACAGTGGCAA-3′ and 5′-GTCGGAGATTCGTAGCTGGA-3′; *IL18*, 5′-TCTTCATTGACCAAGGAAATCGG-3′ and 5′-TCCGGGGTGCATTATCTCTAC-3′; *NLRP3*, 5′-CCACAAGATCGTGAGAAAACCC-3′ and 5′-CGGTCCTATGTGCTCGTCA-3′; *CASP1*, 5′-TTTCCGCAAGGTTCGATTTTCA-3′ and 5′-GGCATCTGCGCTCTACCATC-3′; *IL1R1*, 5′-ATGAAATTGATGTTCGTCCCTGT-3′ and 5′-ACCACGCAATAGTAATGTCCTG-3′; *IL6*, 5′-AAATTCGGTACATCCTCGACGG-3′ and 5′-GGAAGGTTCAGGTTGTTTTCTGC-3′; *TNF*, 5′-ATGAGCACTGAAAGCATGATCC-3′ and 5′-GAGGGCTGATTAGAGAGAGGTC-3′; and *ACTB*, 5′-CATGTACGTTGCTATCCAGGC-3′ and 5′-CTCCTTAATGTCACGCACGAT-3′. Primers used to study *Lpin2* mRNA expression in cells from *Lpin2*$^{-/-}$ and WT mice were as follows: 5′-TTGGGTGATAATGGGGAGCC-3′ and 5′-CTGAGCTGGCCTTTCATTTC-3′.

Electrophysiology

Cells were plated on 12-mm coverslips previously treated with poly-L-lysine (0.01 mg/ml) for 30 min. Patch micropipettes were made from borosilicate glass (2.0 mm OD; WPI) and double pulled (Narishige) to resistances ranging from 5 to 10 MΩ when filled with the internal solution containing 125 mM KCl, 4 mM $MgCl_2$, 10 mM Hepes, 10 mM EGTA, and 5 mM MgATP, pH 7.2. Cells were bathed in an external solution containing 141 mM NaCl, 4.7 mM KCl, 1.2 mM $MgCl_2$, 1.8 mM $CaCl_2$, 10 mM glucose, and 10 mM Hepes, pH 7.4. Cells were voltage-clamped at −80 mV. Ionic currents through $P2X_7R$ were recorded at room temperature using the whole-cell configuration of the patch-clamp technique. Current–voltage relationships were obtained with 1s-ramp protocols from −120 mV to +100 mV applied every 5 s, in control conditions or in the presence of ATP (2 mM) during 1 min. Whole-cell currents were recorded using an Axopatch 200A patch-clamp amplifier (Axon Instruments) filtered at 2 kHz (−3 dB, 4-pole Bessel filter) and sampled at 10 kHz. Recordings were digitized with a Digidata 1200, driven by CLAMPEX 10.2 software (Molecular Devices). Electrophysiological data analyses were performed using Clampfit subroutine of the pClamp software (Axon Instruments) and with Origin 7 software (OriginLab Corporation). In most cases, current amplitude was corrected for cell size variations and expressed as current density (pA/pF), by dividing for cell capacitance values.

K^+ determinations

Intracellular K^+ concentrations were quantified by optical emission spectrometry (Katsnelson et al., 2015). Cells were washed with the K^+-free buffer: 135 mM sodium gluconate, 1.5 mM $CaCl_2$, 1 mM $MgCl_2$, 25 mM Hepes, pH, 7.4. Cells were treated with 2 ml 10% nitric acid for 2 h, and extracted total K^+ content was quantified using an inductively coupled plasma/optical emission spectrometer (ICP/OES) Varian 725-ES (VARIAN Medical Systems, Inc.).

Flow cytometry

Cellular active caspase-1 content was assayed using the fluorescent inhibitor probe FAM-YVAD-FMK to label active

caspase-1 (ImmunoChemistry Technologies) following the manufacturer's instructions. In brief, FAM-YVAD-FMK was added to cells and incubated for 30 min at 37°C. After extensive washes cell fluorescence was quantified by flow cytometry in FL1 (Gallios; Beckman Coulter). Data were analyzed with the software Kaluza version 1.1.

PI uptake was analyzed by incubating cells with 50 µg/ml PI in PBS in the dark for 5 min. Fluorescence was quantified by flow cytometry in FL3. Data were analyzed with Kaluza version 1.1.

Ethidium bromide and Annexin V uptake

Cells on glass-bottom culture dishes (Matteck), were layered with 10 mM Hepes, pH 7.3, 149 mM NaCl, 0.8 mM KCl, 0.6 mM $CaCl_2$, 0.08 mM $MgCl_2$, and 10 mM D-glucose, and imaged using an oil immersion, 63×, 1.4 NA, HCX PL APO CS objective in a confocal microscope at 37°C (TCS SP5X; Leica). Ethidium bromide (20 µM) was added 5 min before stimulation to establish a fluorescence base line, and images were taken at different time points. Fluorescence was excited at 548 nm using a Supercontinium laser and emission was collected over 560 nm. Fluorescence quantification was performed using the ImageJ software (National Institutes of Health).

For Annexin V uptake, cells were layered with a buffer consisting of 10 mM Hepes, 140 mM NaCl, 2.5 mM $CaCl_2$, pH 7.4, to allow proper binding, and 1 µg/ml Annexin V-Cy3 was added 5 min before stimulation. Images were taken every 5 min, as mentioned for ethidium bromide.

Immunostaining

Cells plated over glass coverslips were stimulated, washed with PBS, and fixed with 4% paraformaldehyde and 3% sucrose for 20 min. Cells were then permeabilized with 0.1% Triton X-100 for 2 min and treated with PBS containing 0.5% BSA, 50 mM glycine, and 4% goat serum for 30 min at room temperature. Cells were then washed tree times and incubated with antibodies against ASC diluted 1:50 in PBS plus 0.1% BSA for 1 h. After washing, cells were incubated with Alexa Fluor 488-goat anti rabbit antibodies diluted 1:250 in PBS plus 0.1% BSA for 1 h. Cells were then washed treated with 1 µg/ml DAPI, washed again, and mounted using an antifade solution. Fluorescence was examined using an oil immersion, 63×, 1.4 NA, HCX PL APO CS objective in a Leica TCS SP5X confocal microscope. Alexa Fluor 488 was excited at 485 nm, and fluorescence emission was collected between 508 and 545 nm. DAPI fluorescence was excited with a blue diode at 405 nm and emission was collected between 439 and 475 nm.

Cholesterol determinations

Total cellular cholesterol levels were measured as previously described with a few modifications (Zlatkis et al., 1953). Cells were washed with PBS, and sonicated in water twice for 18 s. Protein concentration was then quantified. Lipids from lysates containing 1 mg protein were extracted with 5 vol of n-hexane:isopropanol (3:2; vol/vol). After centrifugation, the organic phase was recover, evaporated under N_2 atmosphere, and resuspended in chloroform. Lipids were then treated with 1 ml $FeCl_3$ in glacial acetic acid (0.1 mg/ml). After vigorous agitation, the mix was centrifuged at 15,000 *g* for 1 min. Supernatants (0.5 ml) were mixed with 300 ml H_2SO_4 and allowed to react for 30 min, and then absorbance was measured at 560 nm in a spectrometer (VersaMax; Molecular Devices), and the concentration calculated using a standard curve.

Cytotoxicity assay (LDH release)

Cells were stimulated and supernatants were collected and centrifuged at 300 *g* for 10 min. Supernatants were then assayed for LDH activity using a commercially available kit from Roche, following the manufacturer's instructions. Absorbance from the product formazan was measured at 500 nm using a spectrophotometer.

Ethics

Our study with human samples was approved by the Bioethics Committee of the Spanish National Research Council (CSIC) and the Ethics Committee of the University of Valladolid, in accordance with the guidelines established by the Spanish Ministry of Health and the European Union, in conformity with the World Medical Association Declaration of Helsinki. Human samples were provided by the Centro de Hemoterapia y Hemodonación de Castilla y León Biobank (Vallodolid, Spain). Written informed consent was obtained from each donor. The researchers received the samples in an anonymous manner.

Statistics

Data are represented as mean ± SEM, or as mean ± SD. Statistical significance was determined by Student's *t* test, or with one-way ANOVA followed by Tukey's test. $P < 0.05$ was considered statistically significant.

ACKNOWLEDGMENTS

We thank Fernando Martínez, Montserrat Duque, and Yolanda Noriega for their technical assistance.

This work was supported by the Spanish Ministry of Economy and Competitiveness (grants SAF2013-48201-R and BFU2013-45867-R), Instituto de Salud Carlos III (RIC, RD12/0042/0006, Red Heracles), and the Regional Government of Castile and Leon (BIO/VA22/15). G. Lordén, I. Sanjuán-García, N. de Pablo, and I. Alvarez-Miguel were supported by predoctoral fellowships from the Spanish Ministry of Science and Innovation (FPU and FPI programs) and the Regional Government of Castile and Leon. Centro de Investigación Biomédica en Red de Diabetes y Enfermedades Metabólicas is an initiative of Instituto de Salud Carlos III.

The authors declare no competing financial interests.

Author contributions: G. Lordén performed most of the experiments and analyzed the data; I. Sanjuán-García, C. Meana, N. de Pablo, I. Alvarez-Miguel, M.T. Pérez-García, and P. Pelegrín helped with experimentation; J. Balsinde analyzed the data and wrote the manuscript; M.A. Balboa designed the experimentation, analyzed the data, and wrote the manuscript.

Submitted: 31 August 2016
Revised: 23 October 2016
Accepted: 12 December 2016

REFERENCES

Al-Mosawi, Z.S., K.K. Al-Saad, R. Ijadi-Maghsoodi, H.I. El-Shanti, and P.J. Ferguson. 2007. A splice site mutation confirms the role of LPIN2 in Majeed syndrome. *Arthritis Rheum.* 56:960–964. http://dx.doi.org/10.1002/art.22431

Baldassare, J.J., Y. Bi, and C.J. Bellone. 1999. The role of p38 mitogen-activated protein kinase in IL-1 β transcription. *J. Immunol.* 162:5367–5373.

Bartlett, R., L. Stokes, and R. Sluyter. 2014. The P2X7 receptor channel: recent developments and the use of P2X7 antagonists in models of disease. *Pharmacol. Rev.* 66:638–675. http://dx.doi.org/10.1124/pr.113.008003

Basak, C., S.K. Pathak, A. Bhattacharyya, D. Mandal, S. Pathak, and M. Kundu. 2005. NF-κB- and C/EBPβ-driven interleukin-1β gene expression and PAK1-mediated caspase-1 activation play essential roles in interleukin-1β release from *Helicobacter pylori* lipopolysaccharide-stimulated macrophages. *J. Biol. Chem.* 280:4279–4288. http://dx.doi.org/10.1074/jbc.M412820200

Bauernfeind, F.G., G. Horvath, A. Stutz, E.S. Alnemri, K. MacDonald, D. Speert, T. Fernandes-Alnemri, J. Wu, B.G. Monks, K.A. Fitzgerald, et al. 2009. Cutting edge: NF-kappaB activating pattern recognition and cytokine receptors license NLRP3 inflammasome activation by regulating NLRP3 expression. *J. Immunol.* 183:787–791. http://dx.doi.org/10.4049/jimmunol.0901363

Brennan, M.A., and B.T. Cookson. 2000. Salmonella induces macrophage death by caspase-1-dependent necrosis. *Mol. Microbiol.* 38:31–40. http://dx.doi.org/10.1046/j.1365-2958.2000.02103.x

Buisman, H.P., T.H. Steinberg, J. Fischbarg, S.C. Silverstein, S.A. Vogelzang, C. Ince, D.L. Ypey, and P.C. Leijh. 1988. Extracellular ATP induces a large nonselective conductance in macrophage plasma membranes. *Proc. Natl. Acad. Sci. USA.* 85:7988–7992. http://dx.doi.org/10.1073/pnas.85.21.7988

Chuang, S.Y., C.H. Yang, C.C. Chou, Y.P. Chiang, T.H. Chuang, and L.C. Hsu. 2013. TLR-induced PAI-2 expression suppresses IL-1β processing via increasing autophagy and NLRP3 degradation. *Proc. Natl. Acad. Sci. USA.* 110:16079–16084. http://dx.doi.org/10.1073/pnas.1306556110

Compan, V., F. Martín-Sánchez, A. Baroja-Mazo, G. López-Castejón, A.I. Gomez, A. Verkhratsky, D. Brough, and P. Pelegrín. 2015. Apoptosis-associated speck-like protein containing a CARD forms specks but does not activate caspase-1 in the absence of NLRP3 during macrophage swelling. *J. Immunol.* 194:1261–1273. http://dx.doi.org/10.4049/jimmunol.1301676

Di Virgilio, F. 2015. P2X receptors and inflammation. *Curr. Med. Chem.* 22:866–877. http://dx.doi.org/10.2174/0929867322666141210155311

Donkor, J., P. Zhang, S. Wong, L. O'Loughlin, J. Dewald, B.P. Kok, D.N. Brindley, and K. Reue. 2009. A conserved serine residue is required for the phosphatidate phosphatase activity but not the transcriptional coactivator functions of lipin-1 and lipin-2. *J. Biol. Chem.* 284:29968–29978. http://dx.doi.org/10.1074/jbc.M109.023663

Dwyer, J.R., J. Donkor, P. Zhang, L.S. Csaki, L. Vergnes, J.M. Lee, J. Dewald, D.N. Brindley, E. Atti, S. Tetradis, et al. 2012. Mouse lipin-1 and lipin-2 cooperate to maintain glycerolipid homeostasis in liver and aging cerebellum. *Proc. Natl. Acad. Sci. USA.* 109:E2486–E2495. http://dx.doi.org/10.1073/pnas.1205221109

Elliott, E.I., and F.S. Sutterwala. 2015. Initiation and perpetuation of NLRP3 inflammasome activation and assembly. *Immunol. Rev.* 265:35–52. http://dx.doi.org/10.1111/imr.12286

Ferguson, P.J., S. Chen, M.K. Tayeh, L. Ochoa, S.M. Leal, A. Pelet, A. Munnich, S. Lyonnet, H.A. Majeed, and H. El-Shanti. 2005. Homozygous mutations in LPIN2 are responsible for the syndrome of chronic recurrent multifocal osteomyelitis and congenital dyserythropoietic anaemia (Majeed syndrome). *J. Med. Genet.* 42:551–557. http://dx.doi.org/10.1136/jmg.2005.030759

Gu, Y., K. Kuida, H. Tsutsui, G. Ku, K. Hsiao, M.A. Fleming, N. Hayashi, K. Higashino, H. Okamura, K. Nakanishi, et al. 1997. Activation of interferon-gamma inducing factor mediated by interleukin-1β converting enzyme. *Science.* 275:206–209. http://dx.doi.org/10.1126/science.275.5297.206

Han, G.S., W.I. Wu, and G.M. Carman. 2006. The *Saccharomyces cerevisiae* Lipin homolog is a $Mg2^{+}$-dependent phosphatidate phosphatase enzyme. *J. Biol. Chem.* 281:9210–9218. http://dx.doi.org/10.1074/jbc.M600425200

Hara, H., K. Tsuchiya, I. Kawamura, R. Fang, E. Hernandez-Cuellar, Y. Shen, J. Mizuguchi, E. Schweighoffer, V. Tybulewicz, and M. Mitsuyama. 2013. Phosphorylation of the adaptor ASC acts as a molecular switch that controls the formation of speck-like aggregates and inflammasome activity. *Nat. Immunol.* 14:1247–1255. http://dx.doi.org/10.1038/ni.2749

Herlin, T., B. Fiirgaard, M. Bjerre, G. Kerndrup, H. Hasle, X. Bing, and P.J. Ferguson. 2013. Efficacy of anti-IL-1 treatment in Majeed syndrome. *Ann. Rheum. Dis.* 72:410–413. http://dx.doi.org/10.1136/annrheumdis-2012-201818

Hoffman, H.M., J.L. Mueller, D.H. Broide, A.A. Wanderer, and R.D. Kolodner. 2001. Mutation of a new gene encoding a putative pyrin-like protein causes familial cold autoinflammatory syndrome and Muckle-Wells syndrome. *Nat. Genet.* 29:301–305. http://dx.doi.org/10.1038/ng756

Holzinger, D., C. Kessel, A. Omenetti, and M. Gattorno. 2015. From bench to bedside and back again: translational research in autoinflammation. *Nat. Rev. Rheumatol.* 11:573–585. http://dx.doi.org/10.1038/nrrheum.2015.79

Hori, Y., A. Kikuchi, M. Isomura, M. Katayama, Y. Miura, H. Fujioka, K. Kaibuchi, and Y. Takai. 1991. Post-translational modifications of the C-terminal region of the rho protein are important for its interaction with membranes and the stimulatory and inhibitory GDP/GTP exchange proteins. *Oncogene.* 6:515–522.

Katsnelson, M.A., L.G. Rucker, H.M. Russo, and G.R. Dubyak. 2015. K^{+} efflux agonists induce NLRP3 inflammasome activation independently of Ca^{2+} signaling. *J. Immunol.* 194:3937–3952. http://dx.doi.org/10.4049/jimmunol.1402658

Kok, B.P., G. Venkatraman, D. Capatos, and D.N. Brindley. 2012. Unlike two peas in a pod: lipid phosphate phosphatases and phosphatidate phosphatases. *Chem. Rev.* 112:5121–5146. http://dx.doi.org/10.1021/cr200433m

Kuida, K., J.A. Lippke, G. Ku, M.W. Harding, D.J. Livingston, M.S. Su, and R.A. Flavell. 1995. Altered cytokine export and apoptosis in mice deficient in interleukin-1 β converting enzyme. *Science.* 267:2000–2003. http://dx.doi.org/10.1126/science.7535475

Livak, K.J., and T.D. Schmittgen. 2001. Analysis of relative gene expression data using real-time quantitative PCR and the 2(-Delta Delta C(T)) Method. *Methods.* 25:402–408. http://dx.doi.org/10.1006/meth.2001.1262

Lutz, R.J., T.M. McLain, and M. Sinensky. 1992. Feedback inhibition of polyisoprenyl pyrophosphate synthesis from mevalonate in vitro. Implications for protein prenylation. *J. Biol. Chem.* 267:7983–7986.

Majeed, H.A., M. Kalaawi, D. Mohanty, A.S. Teebi, M.F. Tunjekar, F. al-Gharbawy, S.A. Majeed, and A.H. al-Gazzar. 1989. Congenital dyserythropoietic anemia and chronic recurrent multifocal osteomyelitis in three related children and the association with Sweet syndrome in two siblings. *J. Pediatr.* 115:730–734. http://dx.doi.org/10.1016/S0022-3476(89)80650-X

Man, S.M., and T.D. Kanneganti. 2015. Regulation of inflammasome activation. *Immunol. Rev.* 265:6–21. http://dx.doi.org/10.1111/imr.12296

Mariathasan, S., K. Newton, D.M. Monack, D. Vucic, D.M. French, W.P. Lee, M. Roose-Girma, S. Erickson, and V.M. Dixit. 2004. Differential

activation of the inflammasome by caspase-1 adaptors ASC and Ipaf. *Nature.* 430:213–218. http://dx.doi.org/10.1038/nature02664

Mariathasan, S., D.S. Weiss, K. Newton, J. McBride, K. O'Rourke, M. Roose-Girma, W.P. Lee, Y. Weinrauch, D.M. Monack, and V.M. Dixit. 2006. Cryopyrin activates the inflammasome in response to toxins and ATP. *Nature.* 440:228–232. http://dx.doi.org/10.1038/nature04515

Martinon, F., V. Pétrilli, A. Mayor, A. Tardivel, and J. Tschopp. 2006. Gout-associated uric acid crystals activate the NALP3 inflammasome. *Nature.* 440:237–241. http://dx.doi.org/10.1038/nature04516

Meana, C., L. Peña, G. Lordén, E. Esquinas, C. Guijas, M. Valdearcos, J. Balsinde, and M.A. Balboa. 2014. Lipin-1 integrates lipid synthesis with proinflammatory responses during TLR activation in macrophages. *J. Immunol.* 193:4614–4622. http://dx.doi.org/10.4049/jimmunol.1400238

Michel, A.D., and E. Fonfria. 2007. Agonist potency at P2X7 receptors is modulated by structurally diverse lipids. *Br. J. Pharmacol.* 152:523–537. http://dx.doi.org/10.1038/sj.bjp.0707417

Muñoz-Planillo, R., P. Kuffa, G. Martínez-Colón, B.L. Smith, T.M. Rajendiran, and G. Núñez. 2013. K^+ efflux is the common trigger of NLRP3 inflammasome activation by bacterial toxins and particulate matter. *Immunity.* 38:1142–1153. http://dx.doi.org/10.1016/j.immuni.2013.05.016

Navratil, A.R., A.E. Vozenilek, J.A. Cardelli, J.M. Green, M.J. Thomas, M.G. Sorci-Thomas, A.W. Orr, and M.D. Woolard. 2015. Lipin-1 contributes to modified low-density lipoprotein-elicited macrophage pro-inflammatory responses. *Atherosclerosis.* 242:424–432. http://dx.doi.org/10.1016/j.atherosclerosis.2015.08.012

Ochi, H., Y. Hara, M. Tagawa, K. Shinomiya, and Y. Asou. 2010. The roles of TNFR1 in lipopolysaccharide-induced bone loss: dual effects of TNFR1 on bone metabolism via osteoclastogenesis and osteoblast survival. *J. Orthop. Res.* 28:657–663.

Park, Y.H., G. Wood, D.L. Kastner, and J.J. Chae. 2016. Pyrin inflammasome activation and RhoA signaling in the autoinflammatory diseases FMF and HIDS. *Nat. Immunol.* 17:914–921. http://dx.doi.org/10.1038/ni.3457

Perregaux, D., and C.A. Gabel. 1994. Interleukin-1 β maturation and release in response to ATP and nigericin. Evidence that potassium depletion mediated by these agents is a necessary and common feature of their activity. *J. Biol. Chem.* 269:15195–15203.

Péterfy, M., J. Phan, P. Xu, and K. Reue. 2001. Lipodystrophy in the fld mouse results from mutation of a new gene encoding a nuclear protein, lipin. *Nat. Genet.* 27:121–124. http://dx.doi.org/10.1038/83685

Peterson, T.R., S.S. Sengupta, T.E. Harris, A.E. Carmack, S.A. Kang, E. Balderas, D.A. Guertin, K.L. Madden, A.E. Carpenter, B.N. Finck, and D.M. Sabatini. 2011. mTOR complex 1 regulates lipin 1 localization to control the SREBP pathway. *Cell.* 146:408–420. http://dx.doi.org/10.1016/j.cell.2011.06.034

Quartier, P., F. Allantaz, R. Cimaz, P. Pillet, C. Messiaen, C. Bardin, X. Bossuyt, A. Boutten, J. Bienvenu, A. Duquesne, et al. 2011. A multicentre, randomised, double-blind, placebo-controlled trial with the interleukin-1 receptor antagonist anakinra in patients with systemic-onset juvenile idiopathic arthritis (ANAJIS trial). *Ann. Rheum. Dis.* 70:747–754. http://dx.doi.org/10.1136/ard.2010.134254

Rao, A.P., D.B. Gopalakrishna, X. Bing, and P.J. Ferguson. 2016. Phenotypic variability in Majeed syndrome. *J. Rheumatol.* 43:1258–1259. http://dx.doi.org/10.3899/jrheum.151193

Robinson, L.E., M. Shridar, P. Smith, and R.D. Murrell-Lagnado. 2014. Plasma membrane cholesterol as a regulator of human and rodent P2X7 receptor activation and sensitization. *J. Biol. Chem.* 289:31983–31994. http://dx.doi.org/10.1074/jbc.M114.574699

Sakuma, Y., K. Tanaka, M. Suda, Y. Komatsu, A. Yasoda, M. Miura, A. Ozasa, S. Narumiya, Y. Sugimoto, A. Ichikawa, et al. 2000. Impaired bone resorption by lipopolysaccharide in vivo in mice deficient in the prostaglandin E receptor EP4 subtype. *Infect. Immun.* 68:6819–6825. http://dx.doi.org/10.1128/IAI.68.12.6819-6825.2000

Stein, Y., and B. Shapiro. 1957. The synthesis of neutral glycerides by fractions of rat liver homogenates. *Biochim. Biophys. Acta.* 24:197–198. http://dx.doi.org/10.1016/0006-3002(57)90165-8

Surprenant, A., F. Rassendren, E. Kawashima, R.A. North, and G. Buell. 1996. The cytolytic P2Z receptor for extracellular ATP identified as a P2X receptor (P2X7). *Science.* 272:735–738. http://dx.doi.org/10.1126/science.272.5262.735

Udagawa, N., N. Takahashi, T. Akatsu, H. Tanaka, T. Sasaki, T. Nishihara, T. Koga, T.J. Martin, and T. Suda. 1990. Origin of osteoclasts: mature monocytes and macrophages are capable of differentiating into osteoclasts under a suitable microenvironment prepared by bone marrow-derived stromal cells. *Proc. Natl. Acad. Sci. USA.* 87:7260–7264. http://dx.doi.org/10.1073/pnas.87.18.7260

Valdearcos, M., E. Esquinas, C. Meana, L. Gil-de-Gómez, C. Guijas, J. Balsinde, and M.A. Balboa. 2011. Subcellular localization and role of lipin-1 in human macrophages. *J. Immunol.* 186:6004–6013. http://dx.doi.org/10.4049/jimmunol.1003279

Valdearcos, M., E. Esquinas, C. Meana, L. Peña, L. Gil-de-Gómez, J. Balsinde, and M.A. Balboa. 2012. Lipin-2 reduces proinflammatory signaling induced by saturated fatty acids in macrophages. *J. Biol. Chem.* 287:10894–10904. http://dx.doi.org/10.1074/jbc.M112.342915

Xu, H., J. Yang, W. Gao, L. Li, P. Li, L. Zhang, Y.N. Gong, X. Peng, J.J. Xi, S. Chen, et al. 2014. Innate immune sensing of bacterial modifications of Rho GTPases by the Pyrin inflammasome. *Nature.* 513:237–241. http://dx.doi.org/10.1038/nature13449

Zlatkis, A., B. Zak, and A.J. Boyle. 1953. A new method for the direct determination of serum cholesterol. *J. Lab. Clin. Med.* 41:486–492.